AD-A139 921 LIMITS OF PATTERN DISCRIMINATION IN HUMAN VISION(U) 1/1
YALE UNIV NEW HAVEN CT DEPT OF OPHTHALOMOLOGY AND
VISUAL SCIENCE J HIRSCH 30 JAN 84 AFOSR-TR-84-0183
UNCLASSIFIED F49620-83-C-0026 F/G 5/10 NL

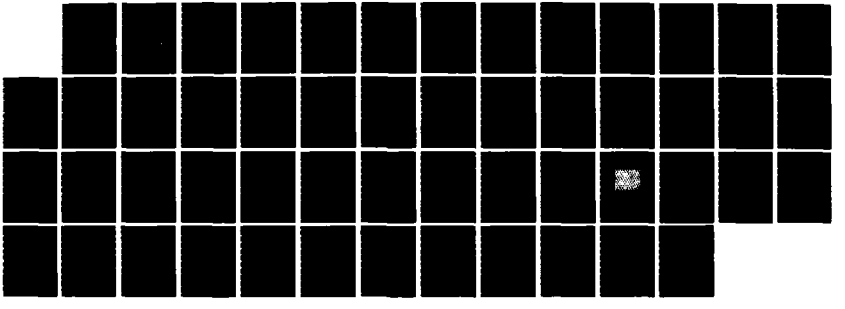

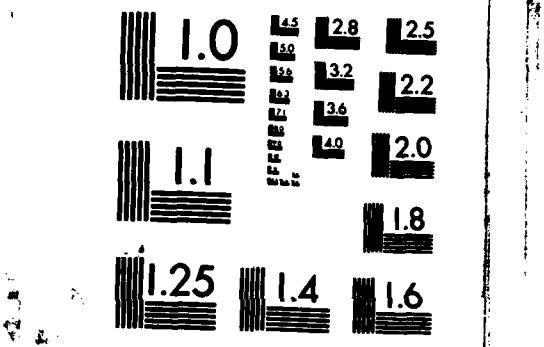

MICROCOPY RESOLUTION TEST CHART
NATIONAL BUREAU OF STANDARDS-1963-A

UNCLASSIFIED

SECURITY CLASSIFICATION OF THIS PAGE (When Data Entered)

REPORT DOCUMENTATION PAGE		READ INSTRUCTIONS BEFORE COMPLETING FORM
1. REPORT NUMBER AFOSR-TR- 84-0183	2. GOVT ACCESSION NO.	3. RECIPIENT'S CATALOG NUMBER
4. TITLE (and Subtitle) Limits of Pattern Discrimination in Human Vision		5. TYPE OF REPORT & PERIOD COVERED Annual Report 6. PERFORMING ORG. REPORT NUMBER
7. AUTHOR(s) Joy Hirsch, Ph.D.		8. CONTRACT OR GRANT NUMBER(s) F49620-83-C-0026
9. PERFORMING ORGANIZATION NAME AND ADDRESS Yale University School of Medicine Dept. of Ophthalmology and Visual Science 310 Cedar Street, BML 219 // New Haven, CT 06510		10. PROGRAM ELEMENT, PROJECT, TASK AREA & WORK UNIT NUMBERS 61102F 2313/A5
11. CONTROLLING OFFICE NAME AND ADDRESS Air Force Office of Scientific Research/NL Bolling AFB, DC 20332		12. REPORT DATE 30 Jan 84 13. NUMBER OF PAGES 49
14. MONITORING AGENCY NAME & ADDRESS(if different from Controlling Office)		15. SECURITY CLASS. (of this report) UNCLASSIFIED 15a. DECLASSIFICATION/DOWNGRADING SCHEDULE

16. DISTRIBUTION STATEMENT (of this Report)

Approved for public release;
distribution unlimited.

17. DISTRIBUTION STATEMENT (of the abstract entered in Block 20, if different from Report)

DTIC ELECTE APR 1 0 1984 S D A

18. SUPPLEMENTARY NOTES

19. KEY WORDS (Continue on reverse side if necessary and identify by block number)

Visual discrimination, hyperacuity, photoreceptor lattice

20. ABSTRACT (Continue on reverse side if necessary and identify by block number)

The studies reported in Annual Technical Report 1 were designed to probe various aspects of spatial pattern discrimination. Several important findings have emerged allowing limits of pattern discrimination to be related to structural properties of the photoreceptor lattice. First, our findings have suggested that spatial frequency discrimination exceeds resolution of the photoreceptor mosaic for spatial frequencies above approximately 4 c/deg, thus spatial frequency

DD FORM 1 JAN 73 1473 EDITION OF 1 NOV 65 IS OBSOLETE

UNCLASSIFIED

SECURITY CLASSIFICATION OF THIS PAGE (When Data Entered)

discrimination qualifies as a hyperacuity task. Further, spatial frequency discrimination was not a smooth function of spatial frequency, but rather showed a regularly segmented structure that appeared to be related to foveal photoreceptor center-to-center spacing. This result suggests that the photoreceptor lattice could be the primary geometrical instrument for estimating distance or separations between stimulus features.

In addition to our study of spatial discrimination, we have developed a technique to study the structural quality of a retinal mosaic by digitizing the foveal photoreceptor lattice of a primate (Macacca fascicularis). Our analyses of the foveal region has revealed a very high quality hexagonal lattice with a correlation length of at least 130 photoreceptors. These results confirm that the photoreceptor lattice is constructed with sufficient structural quality to provide a source of geometrical information reflected in spatial discrimination tasks.

A logical consequence of the above argument that cortical image processing for spatial discrimination tasks may reflect the one dimensional organization (center-to-center spacing) of the retinal photoreceptor lattice is that the same processing also reflects the two dimensional structure (hexagonal) of the photoreceptor lattice. A study of spatial frequency discrimination and vernier acuity as a function of orientation showed a substantial 60° period suggesting that indeed such a model was plausible. We have proposed a specific model (referred to as the Scaled Lattice Model of Spatial Vision) that relates spatial frequency discrimination and the photoreceptor lattice. Briefly, the model suggests that spatial intervals are measured by counting points on the neural lattice between the relevant stimuli. There exist multiple neural scales each related to the fundamental photoreceptor unit size. A scale selection mechanism exists that determines the sampling scale and interpolation factor such that the effective lattice spacing is roughly proportional to the spatial scale of the measurement.

The generalizability of the Scaled Lattice Model was tested in an experiment where our measurements were extended to frequencies as low as 0.3 c/deg. For this new range of spatial frequencies (0.3 - 2 c/deg) we find a similar segmented structure with ε equal to about 0.056 deg or 7 times the foveal photoreceptor spacing. We attribute this to spatial sampling by an array of retinal receptive fields (which we call spatial sampling fields), and interpret this finding as support for the fundamental contribution of the photoreceptor lattice to spatial discrimination.

Annual Technical Report 1

United States Air Force
Air Force Office of Scientific Research

Principal Investigator:

Joy Hirsch, Ph.D.
Yale University
School of Medicine
Dept. of Ophthalmology and Visual Science
310 Cedar Street BML 219
New Haven, CT 06510

Title of Research Program:

Limits of Pattern Discrimination in Human Vision
F49620-83-C-0026

Period of Report:
1 Jan 83 to 30 Jan 84

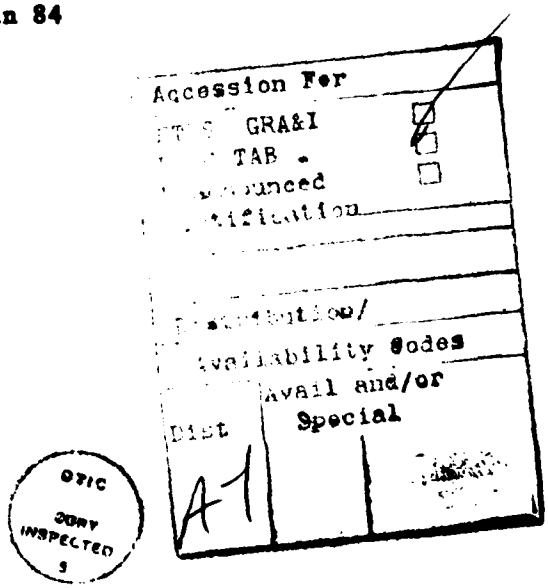

Annual Technical Report 1

United States Air Force
Air Force Office of Scientific Research

Limits of Pattern Discrimination in Human Vision

1 Jan 83 to 30 Jan 84

TABLE OF CONTENTS

Joy Hirsch
F49620-83-C-0026

ABSTRACT

Limits of Pattern Discrimination in Human Vision

The studies reported in Annual Technical Report 1 were designed to probe various aspects of spatial pattern discrimination. Several important findings have emerged allowing limits of pattern discrimination to be related to structural properties of the photoreceptor lattice. First, our findings have suggested that spatial frequency discrimination exceeds resolution of the photoreceptor mosaic for spatial frequencies above approxomately 4 c/deg, thus spatial frequency discrimination qualifies as a hyperacuity task. Further, spatial frequency discrimination was not a smooth function of spatial frequencv, but rather showed a regularly segmented structure that appeared to be related to foveal photoreceptor center-to-center spacing. This result suggests that the photoreceptor lattice could be the primary geometrical instrument for estimating distance or separations between stimulus features.

In addition to our study of spatial discrimination, we have developed a technique to study the structural quality of a retinal mosaic by digitizing the foveal photoreceptor lattice of a primate (Macacca fascicularis). Our analyses of the foveal region has revealed a very high quality hexagonal lattice with a correlation length of at least 130 photoreceptors. These results confirm that the photoreceptor lattice is constructed with sufficient structural quality to provide a source of geometrical information reflected in spatial discrimination tasks.

A logical consequence of the above argument that cortical image processing for spatial discrimination tasks may reflect the one dimensional organization (center-to-center spacing) of the retinal photoreceptor lattice is that the same processing also reflects the two dimensional structure (hexagonal) of the photoreceptor lattice. A study of spatial frequency discrimination and vernier acuity as a function of orientation showed a substantial 60 period suggesting that indeed such a model was plausible. We have proposed a specific model (referred to as the Scaled Lattice Model of Spatial Vision) that relates spatial frequency discrimination and the photoreceptor lattice. Briefly, the model suggests that spatial intervals are measured by counting points on the neural lattice between the relevant stimuli. There exist multiple neural scales each related to the fundamental photoreceptor unit size. A scale selection mechanism exists that determines the sampling scale and interpolation factor such that the effective lattice spacing is roughly proportional to the spatial scale of the measurement.

The generalizability of the Scaled Lattice Model was tested in an experiment where our measurements were extended to frequencies as low as 0.3 c/deg. For this new range of spatial frequencies (0.3 - 2 c/deg) we find a similar segmented structure with ε equal to about 0.056 deg or 7 times the foveal photoreceptor spacing. We attribute this to spatial sampling by an array of retinal receptive fields (which we call spatial sampling fields), and interpret this finding as support for the fundamental contribution of the photoreceptor lattice to spatial discrimination.

A. OBJECTIVES OF THE RESEARCH EFFORT

1. To study how the limits of spatial frequency discrimination are related to hyperacuity performance and neural interpolation,

2. To investigate the quality of the primate photoreceptor lattice and relate the structural properties of the foveal retinal mosaic to the 'neural metric' employed in hyperacuity tasks,

3. To study how spatial frequency discrimination varies as a function of stimulus orientation,

4. To determine the limits of spatial frequency discrimination for very low spatial frequencies,

5. To develop a model of spatial discrimination that accounts for the above findings.

B. STATUS OF THE RESEARCH EFFORT

1. LIMITS OF SPATIAL FREQUENCY DISCRIMINATION AND RELATION TO HYPERACUITY PERFORMANCE.

The accuracy with which the human visual system is able to estimate positions of lines (as in the case of vernier acuity) exceeds the resolution of the photoreceptor mosaic. This extraordinary sense of image position requires some form of neural interpolation in order to achieve such a fine grained representation.[1,2,3] In recent years much attention has been given to the spatial frequency properties of the eye. However, the limits of suprathreshold frequency discrimination have not previously been related to the limits of separation discrimination. In this study we investigate the role of neural interpolation in spatial frequency discrimination tasks. We find that the limits of spatial frequency discrimination require resolution finer than the size of a single photoreceptor, and that performance on this task is very similar to performance on separation discrimination tasks. We also find that spatial frequency discrimination is not a smooth function of frequency, but rather has a regularly segmented structure.

METHODS AND PROCEDURE

Stimuli were vertical sinusoidal spatial frequency gratings electronically generated on the face of a CRT (Tektronix 606, P31 phosphor). The gratings were calculated by a PDP 11/03 computer and stored in digital display generating hardware.

Sessions were controlled by the laboratory computer, and the data analysis followed each experimental session. The data were gathered over a period of 18 months in irregular order.

The observer initiated a trial by pressing a ready key. A trial consisted of a reference grating presented for 1.5 sec, an interstimulus interval of .75 sec, and a test grating presented for 1.5 sec. All stimuli were stationary with abrupt on and offsets, and the phases of both the test and reference gratings were independently randomized on each trial. Onsets of both reference and test gratings were cued by a tone. A response period followed the test stimulus and was indicated by a beep and an LED alphanumeric display located to the side of the screen.

The observer's task was to decide if the test grating had a higher or a lower spatial frequency than the reference grating. A two alternative forced choice method was employed where the observer signaled a 'high' or 'low' response by pressing the appropriate key on a response panel. Following each response a synthesized voice unit (Votrax VSK) replied either 'high', 'low', or 'same' indicating whether the test grating presented on that trial had been a higher spatial frequency, a lower spatial frequency, or the same spatial frequency as the reference grating.

Seven test gratings were employed during each session. Three were of lower spatial frequency than the reference grating, three were of higher spatial frequency than the reference, and one was the same spatial frequency as the reference. Test grating frequencies were chosen symmetrically about the reference frequency. All reference gratings were presented at 30% contrast. Prior to the sessions, a contrast matching experiment was done so that each test grating had the same apparent contrast as the reference grating.[4] In addition, on each trial the contrasts of both the test and reference gratings were given small random variations (between $\pm$ 1 db) to further ensure that no contrast cues existed. All test gratings were randomized and presented with equal probabilities. Each test grating was presented 50 times. A session consisted of 350 trials plus 20 initial practice trials that were excluded from the data analysis.

The probability of a 'high' response was fit to a cumulative normal distribution described by two parameters, f_c and Δf. The value of f_c is the frequency at which the probability of a 'high' response is .50, and Δf, the just discriminable difference (jnd) in spatial frequency, is proportional to the width of the normal distribution with a constant scale factor chosen so that the probability of a correct response is .75 when $f-f_c$ equals Δf. (Δf equals .68 times the standard deviation of the fitted normal distribution.) The fit was made using the method of maximum likelihood and also yielded estimates of the statistical errors for both parameters. The estimated error bars were verified by replicating a number of points over time. Chisquared values calculated for the fits indicated good agreement between the fit and the data in all cases, and f_c did not differ significantly from the reference frequency.

RESULTS

Discrimination as a function of spatial frequency

Three observers (JH, BA, and MM) with unimpaired vision participated in the experiment. Data from each are shown in Figures 1a, 1b, and 1c respectively.

- - - - - - - - - - -

FIG 1

- - - - - - - - - - -

Values of $\Delta f/f$ (where Δf is defined above and f is the reference frequency) are plotted against the reference frequency. Each point represents one session and errors on each point are estimates from the fitting procedure. The data are clearly not a smooth function of frequency but rather show a segmented structure for all observers. Further, the data are not well fit by a single straight line (chisquared confidence levels less than .05 in all three cases).

Examination of the data yields several significant characteristics of the $\Delta f/f$ vs f function. First, the $\Delta f/f$ function can be divided into several segments. The segments occur at approximately the same place for all observers, and are separated by transition regions where $\Delta f/f$ falls rapidly with spatial frequency. The transitions appear nearly regularly spaced in spatial frequency, repeating about every four cycles/deg. Peak values of $\Delta f/f$ are about the same for each segment across all observers, with a value of approximately .032. Within each segment $\Delta f/f$ rises with spatial frequency (following the transition), and the points are clustered around straight lines drawn through the origin. These lines are drawn in Figures 1a, 1b, and 1c, and the derivations are discussed below. The slopes of these lines vary systematically from segment to segment. Disregarding the segmentation, it can be seen from Figure 1 that $\Delta f/f$ is essentially independent of spatial frequency. This observation suggests that over the range of spatial frequencies studied the visual system on the average achieves a resolution which is a constant fraction (approximately .025) of the size of the relevant visual characteristic.

Discrimination as a function of field size

In a second set of measurements all gratings were presented as described above except that the extent of sinusoidal modulation for both test and reference gratings in a particular session was restricted to a region of constant angular width less than the full screen. The phases were randomized as described above and the modulation was abruptly reduced to zero outside the display region. Both test and reference gratings remained centered in the four degree field. Figure 2 shows $\Delta f/f$ as a function of the number of cycles in the reference grating for observer BA

- - - - - - - - - - -

FIG 2

- - - - - - - - - - -

and spatial frequencies of 4, 8, and 12 cycles/deg. Similar results were found for observer JH. In all cases it can be seen that the $\Delta f/f$ function is independent of field size until the field size becomes less than two cycles. The scatter in the data for field sizes of two cycles and above is consistent with the error bars on each point. We interpret this as evidence that the spatial frequency discrimination was in fact done by measurement of the separation between two visual features separated by exactly one spatial cycle. In particular, if the task were based on measurement of the distance between two successive peaks, performance would degrade rapidly as field size became less than two cycles because a random sample of a sine wave becomes increasingly less likely to contain two intact peaks as the sample width decreases below two cycles. A sample containing only one cycle cannot contain two intact peaks.

Discrimination of separations between line pairs

The assumption that discrimination between spatial frequency gratings is primarily dependent upon the distance between two luminance peaks was further tested in a third experiment. This experiment was similar to the spatial frequency discrimination experiments described above except that a single pair of very thin vertical lines on a dark background was presented instead of a spatial frequency grating. The task for the observer was to decide if the separation between the test pair of lines was greater or less than the separation between the reference pair of lines. Deviations of test separations from reference separations were controlled to an accuracy of better than 10^{-4} degrees, and the center of each pair of lines was independently randomized around the center of the display by $\pm$ 1/4 of the reference separation. In all other respects, this experiment was the same as the spatial frequency experiments. Data from each session were analyzed as above to obtain estimates of the center separation, the jnd in separation Δs, and the error on each. The results for this experiment are shown for observer JH in Figure 3. The fractional resolution in separation, $\Delta s/s$, is plotted against the inverse of reference separation, $1/s$. Both axes of this graph are dimensionally

- - - - - - - - - - -

FIG 3

- - - - - - - - - - -

directly comparable to those of Figure 1. The similarity between the data in Figures 1 and 3 is striking. The separation discrimination data clearly shows the same segmentation as was observed in the spatial frequency discrimination data. The only significant disagreement between the two sets of data is in the region between 3 and 4 deg^{-1} where the separation discrimination data makes the transition between the first and second segments earlier and somewhat more gradually than the frequency discrimination data. Similar results were found for another observer, JM. It is interesting that greater differences were not observed especially in the low frequency region where the curvature of the peaks for the line stimuli (determined by the line spread function) was considerably greater than the curvature of the corresponding sinusoidal stimuli.

Spatial frequency discrimination as a width discrimination task

Given the assumption that the critical visual feature for the sinusoidal spatial frequency discrimination task was the separation between two successive peaks, we can convert from the jnd in spatial frequency (Δf) to a jnd in visual angle (Δs). The separation between cycles in degrees is given by

$$s = 1/f \qquad (1)$$

where f is the spatial frequency of the reference grating. Differentiating equation 1 shows that

$$\Delta s = \Delta f / f^2 \quad . \qquad (2)$$

It is also useful to note that the fractional resolution in spatial frequency is equal to the fractional resolution in angular separation. This is shown by rewriting equation 2 in the form:

$$\Delta f / f = \Delta s / s \quad . \qquad (2.1)$$

Angular resolution for discrimination tasks is less than the spacing between photoreceptors

In Figure 4a the spatial frequency data for observer JH are replotted in terms of Δs and compared to the separation discrimination data shown in 4b. Also shown in Figure 4b are results of a similar line pair experiment previously reported by

- - - - - - - - - - -

FIG 4

- - - - - - - - - - -

Westheimer[2] (open symbols) which are consistent with our observations. From this figure it can be seen that the angular resolution Δs for both tasks is much smaller than the spacing between photoreceptors for medium and high spatial frequencies. (As a point of reference, the size of a photoreceptor is estimated to be about 30 secs of arc or .008 degrees[2].)

As noted above, the data in Figures 1 and 3 cluster about straight lines drawn through the origin in the $\Delta f/f$ vs f plane. Rewriting equation 2 in the form

$$\Delta f/f = \Delta s * f \qquad (2.2)$$

shows that such lines represent regions of constant Δs. These lines are transformed to the horizontal dashed lines in Figure 4. We see that Δs as a function of f has a step-like form and that the segments described in Figures 1 and 3 are regions of constant Δs. The values of Δs are very nearly the same for the frequency discrimination data and the separation discrimination data.

DISCUSSION

A key argument made above is that the sinusoidal frequency discrimination task was done by locating specific features of the stimulus separated by exactly one cycle, presumably two successive peaks, and measuring the distance between them. The evidence for this is found in the field size and line pair separation discrimination results. The field size data clearly show that the task required more than 1/2 cycle and less than two cycles of the spatial frequency grating. More decisive evidence is shown in Figure 4 where we see that the spatial frequency discrimination results and the separation discrimination results are almost identical when related by this assumption (equations 1 and 2). We have not shown conclusively that the relevant features for the sinusoids are two successive peaks. However, we have shown that the task involved two well-defined features separated by exactly one cycle. The only possibilities for the relevant features are two successive peaks or two successive valleys since 'zero crossings' are separated by only one half cycle and 'zero' is not well defined (particularly in the field size experiments) since there was generally not an integral number of cycles in the display. Luminance peaks (or valleys) occur in essentially all visual stimuli, and a mechanism which locates these features would be generally applicable. Westheimer and McKee have shown that hyperacuity comparable to that reported here occurs in a wide variety of visual tasks and has little or no dependence on the exact stimulus employed.[5,6]

These results would be difficult to interpret in terms of a global model where the detector involves several or many cycles. In particular, the Fourier spectrum of a sine wave sample consisting of only one cycle is very broad with a width of 50 to 100% of the center frequency, and a line pair is not usefully described in terms of its Fourier spectrum. Hence, the similarity of the results would be difficult to explain in terms of their spatial frequency content. However, a model dependent upon the separation between the luminance peaks of the stimulus would predict the same results for both experiments. We also note that once the field size has exceeded two cycles, no further improvement is observed in discrimination. If any form of non-local summation existed, it would be expected that Δf would decrease with increasing field size. Even simple averaging of the widths of many separately measured cycles would lead to decreases in Δf proportional to $1/\sqrt{\text{field size}}$. The visual system apparently does not exploit non-local information for this discrimination task.

2. QUALITY OF THE PRIMATE PHOTORECEPTOR LATTICE AND SPATIAL DISCRIMINATION

There is a growing recognition that the photoreceptor lattice must play a fundamental role in spatial vision.[7,8,9] The question of how accurately the photoreceptors are placed in the lattice then becomes of considerable importance, and two quite different views of the consequences of imperfections in the lattice have been proposed. We have recently presented evidence suggesting that spatial intervals are measured by counting points in a cortical lattice which is derived from the photoreceptor lattice. From this point of view, the photoreceptor lattice is the basic geometrical instrument for measuring distances and any randomness in the spacing of photoreceptors will limit the accuracy with which the measurements can be made.

METHODS

To study the question of photoreceptor lattice quality we have analyzed the foveal cone mosaic from an adult primate (Macaca fascicularis) using an electron micrograph of a section taken tangent to the external limiting membrane (ELM) close to its scleral side (Miller, 1979).[10] Our analysis is based on measurements of the positions of the centers of about 100 cone inner segments in the central fovea (Fig. 5). This lattice was chosen for analysis rather than that published by

- - - - - - - - - - -

FIG 5

- - - - - - - - - - -

Polyak (1957) and studied by Yellott (1982) because the Polyak lattice is a photograph of a whole mount that appears to be focused near the level of the outer segments. The outer segment locations are irrelevant for positional analysis since the outer segments are basically light guides for photons that enter the cones at the inner segments. The outer segments may also be subject to substantial positional distortion since they are embedded in a semifluid extracellular matrix. In contrast, the positions of the inner segments are fixed at the ELM by desmosomes, after which they taper and increase in refractive index to become light guides, providing the mechanism by which the cones form separate optical channels. Thus the inner segment at the ELM is the spatial aperture of the cone for its photon catching function and its position specifies cone location for the purpose

of image reconstruction. We further note that the Miller lattice displays clearly higher spatial quality than the Polyak lattice. Given the unlikelihood of accidentally introducing order into an initially disordered lattice, the more orderly lattice must be more representative of the intact retina.

RESULTS

Fig. 6a is a histogram of the distances between the centers of all pairs of

FIG 6

photoreceptors in our sample. There is a very distinct peak corresponding to the nearest neighbor distance (which we call ring 1). The rms width of the peak (standard deviation of the nearest neighbor distance) is .077 times the mean separation between nearest neighbor photoreceptors and drops to .070 when the contribution from our measurement error is removed. This is comparable to the maximum tolerable spacing error (.078) estimated below from human psychophysical results.

Fig. 6b shows a histogram of the angles between the horizontal axis and the lines connecting the center of each photoreceptor to the center of its nearest neighbors where nearest neighbors are defined as any pair whose center to center separation is less than the maximum nearest neighbor distance shown in 2a. This figure shows a well defined set of directions with hexagonal symmetry (60° spacing) which determine the orientation of the lattice, and is consistent with previous qualitative observations of retinal structure.[11,12] (It has been pointed out to us that the packing of the lattice approximates a hexagonal tessellation with the centers of the receptors forming a triangular lattice.)

By specifying the mean nearest neighbor distance and orientation of the lattice we have fully determined the basis vectors for the lattice. (See Kittel, 1971, for a discussion of crystal structure.)[13] We then make the following calculations. For each photoreceptor we take its center to be the origin and use the nearest neighbor distance cut determined from Fig. 6 to locate its nearest neighbors. We then measure the difference between expected and actual positions for the photoreceptors just assigned to the ring of nearest neighbors assuming a perfect hexagonal lattice with the basis vectors determined above. The nearest neighbor distance cut is then used again to move out from the nearest neighbors to the ring of second nearest neighbors and again we measure the error in actual position versus the expected position for a perfect hexagonal lattice centered on the original photoreceptor. We continue this process until all photoreceptors have been assigned to some ring and their errors computed. The process is then repeated with a new photoreceptor at the origin. Fig 7 shows a graph of the variance (mean square error) in relative position as a function of ring number. The data have been normalized so that the mean nearest neighbor photoreceptor distance (ring 1)

FIG 7

is 1.0. We plot separately the components of variance parallel and perpendicular to the line which joined the photoreceptor at the origin and the one being tested. The parallel component corresponds to errors in separation while the perpendicular component corresponds to errors in orientation. The variance increases linearly with distance (ring number), consistent with accumulating uncorrelated errors, and the parameters of the best fit straight lines are given in Table I. Measurement error and jitter in the lattice (discussed below) would lead to a positive y intercept and appear to be small.

Table I

If we define the positional correlation length of the lattice as the distance between two lattice points at which the rms spacing error equals the lattice spacing, then the correlation length for the parallel component is 178 $\pm$ 7 photoreceptors and for the perpendicular component the correlation length is 133 $\pm$ 5 photoreceptors.

Sources of error and limitations of the analysis.

While these results establish that the photoreceptor lattice is highly accurate, there is a potential problem with the data that may have caused the degree of error to be severely overestimated. Close inspection of the lattice in Fig. 5 leaves the impression that the lines formed by nearest neighbor photoreceptors are not perfectly straight but rather possess a slight degree of curvature. Numerical analysis confirms that this is indeed the case and that the lattice is systematically distorted. Further, these systematic errors contribute substantially to the increase in variance with distance shown in Fig. 7. If these distortions were introduced in the preparation process they should be removed from the data, and one might even argue that, regardless of origin, systematic errors are correctible and should not be included in this analysis.

We have attempted to correct for this problem in a number of ways and conclude that systematic distortion accounts for roughly half of the slope in Fig. 7 while decreasing the ring 1 variances only slightly. (Jitter in the lattice is then significant). We estimate that with the systematic distortions removed, the correlation lengths may be as much as 400 for the parallel and 200 for the perpendicular components respectively, with the psychophysical limit intersecting the parallel variance at about 2.5 photoreceptors. Thus we believe the above estimates of correlation length are conservative.

CONCLUSION

We have quantitatively analysed the spatial quality of a primate foveal cone lattice. We find that it is a high quality hexagonal lattice with a correlation length of at least 130 photoreceptors over spans of tens of photoreceptors. We find that there is not sufficient disorder in the foveal lattice to prevent aliasing. Rather the photoreceptor lattice seems to be constructed with sufficient accuracy so that it can serve as the fundamental metric for spatial vision even in hyperacuity tasks. This suggests there is no need for any visual mechanism to

measure the true photoreceptor positions and the burden of spatial calibration falls on the developmental processes involved in the formation of the photoreceptor lattice. The measurements reported here combined with our previous psychophysical results suggest a model of spatial vision in which the photoreceptor lattice is the sole geometrical element with all other elements being topological.

3. SPATIAL FREQUENCY DISCRIMINATION AS A FUNCTION OF STIMULUS ORIENTATION.

Recently we reported that discriminating between spatial frequencies of suprathreshold sinusoidal gratings near and above four cycles/degree (c/deg) is a task involving spatial hyperacuity, angular resolutions finer than the center-to-center spacing of foveal photoreceptors[9]. Further, the magnitudes of the hyperacuity thresholds were related to the center-to-center spacing of photoreceptors. We suggested that this relationship was due to a cortical representation of the image that directly reflected the organization of the retinal photoreceptor lattice. A logical consequence of this argument is that the two dimensional properties of the cortical mechanisms which process spatial information should also reflect the two dimensional organization of the photoreceptor lattice. In this paper we report evidence that this is indeed the case and that the orientation dependence of two different tasks involving hyperacuity contains a component with hexagonal symmetry (period = 60°), presumably reflecting the hexagonal packing of photoreceptors.[10] In addition, we find that the orientation dependence of vernier offset discrimination contains another component with square symmetry (period = 90°) and that the phases of the components of the two tasks are not arbitrary. We present a specific model for the origin of the hexagonal component.

METHODS

Two different tasks were employed: discriminating between spatial frequencies of suprathreshold sinusoidal gratings and discriminating the direction of the vernier offset of two narrow lines. In both experiments stimuli were electronically generated on an oscilloscope screen (Tektronix 606). A single experimental session measured a threshold for a particular orientation, so that the orientation of all patterns remained constant during each session. Different orientations were set for different sessions by physically rotating the display, which was a 4 deg circular field set in a 12 deg circular surround matched in hue and brightness to the central display field. The orientation for each session was chosen in an irregular order separately for each observer and task. Observers in both experiments were seated 150 cm from the stimulus screen. Head stabilization was achieved by a chin and forehead rest modified to also include bilateral head supports.

In the case of the spatial frequency discrimination experiments sinusoidal gratings were displayed at 30% contrast. Each session employed a constant reference frequency and a set of nine test frequencies chosen symmetrically around the reference. Each trial consisted of a .75 sec presentation of the reference grating, a .75 sec interstimulus interval, and a .75 sec presentation of one of the test gratings. Spatial phase was randomized on each presentation for both reference and test gratings independently. The order of test presentations was randomized according to the method of constant stimuli and each test pattern was

presented 50 times. Following each trial the observer indicated whether the test frequency was higher or lower than the reference and was given feedback by synthesized voice indicating the true relationship. The probability distributions were fit to a cumulative normal distribution and the just noticeable difference (jnd) in frequency (Δf) was defined as the change in frequency necessary to increase the probability of a correct response from .5 to .75. The fitting procedure also estimated the statistical error in Δf. Full details of the spatial frequency discrimination experiments have previously been reported.[9]

The vernier offset experiments were identical in all respects to the spatial frequency discrimination experiments except that each presentation of a grating was replaced by the presentation of a vernier discrimination target consisting of two narrow line segments each .25 deg long separated by a gap of .25 deg. For the reference pattern the two lines were colinear while the test patterns had small perpendicular offsets. The overall position of the target was randomly offset from the center of the screen for the test and reference patterns independently on each trial by up to .2 deg. The task of the observer was to determine the direction of the vernier offset, and the jnd in offset (Δo) was determined as for Δf. Orientation for different sessions was again varied by physically rotating the screen.

Two well-practiced observers participated in this experiment. Neither wore any optical correction during the experiment. Visual acuity for JH was 20/20 in each eye with no astigmatism, and the axial length for her right eye was 22.2 mm. Visual acuity for SC was also 20/20 in each eye with no astigmatism. The axial length for her right eye was 22.1 mm. Neither observer had any history of eye disease, and we assume both observers are representative of normal vision.

RESULTS

The results of the spatial frequency experiments are shown in Fig. 8 for observer SC at a reference frequency of 4.0 c/deg and for observer JH at a reference frequency of 4.5 c/deg. As discussed below these reference frequencies

- - - - - - - - - - -

FIG 8

- - - - - - - - - - -

were chosen in the expectation (derived from our model of spatial-frequency discrimination) that they would maximize the hexagonal orientation effects predicted above. The figure shows the fractional jnd in spatial frequency $\Delta f/f$ (f is the reference frequency) plotted against the orientation of the grating where an orientation of 0° corresponds to the usual vertical grating. The data are clearly not constant but show significant variation with orientation.[14] Multiple data points are repeated measurements over time and show good stability.[15] The curves are fits to the data and are discussed in detail below.

Fig. 9 shows the results for the vernier discrimination experiments for the

- - - - - - - - - - -

FIG 9

- - - - - - - - - - -

same two observers with the gap in the vernier target equal to .25 deg, also chosen in the expectation of a maximal hexagonal effect. The vernier offset thresholds are plotted against the orientation of the stimulus with an orientation of 90° corresponding to the usual vertical vernier target. This choice is not arbitrary but is required to align the vernier discrimination data with the spatial frequency discrimination data. The vernier thresholds also clearly depend on orientation and are stable over time as indicated by multiple determinations.

DATA ANALYSIS

We find that the orientation dependence of the data presented above consists of the sum of two periodic components, one with hexagonal symmetry (60° period) and harmonics thereof and the other with square symmetry (90° period) and its harmonics. The most general form for a component with period L is

$$f(x) = \sum_{N=1}^{M} a_N \cos(2\pi N x/L) + b_N \sin(2\pi N x/L). \quad (1)$$

However, we also require that there be no difference between positive and negative rotation leading to the more restricted form:

$$f(x) = \sum_{N=1}^{M} a_N \cos(2\pi N (x-x_0)/L) \quad (2)$$

which has even symmetry around some unknown symmetry axis x_0. The value of M (the number of harmonics) is in principle determined by sampling requirements but in practice M = 2 suffices for all the data reported here except for the JH vernier discrimination data which requires some higher harmonics of the square component to achieve a good fit.

Table II shows the results of fitting the data in Fig 8 and Fig 9 to four

Table II

different models of orientation dependence: (1) no orientation dependence, (2) the orientation dependence consists of a hexagonal component only, (3) a square component only, and (4) the sum of a square and hexagonal component. The chi squared (X^2) values, degrees of freedom (df) and levels of confidence for the fits are listed in the table. A large chi squared indicates that the deviations of the data from the model are larger than can be accounted for by the error bars. Both frequency discrimination observers have marginally acceptable fits for the hexagonal only model and good fits for the hexagonal + square model while the square only model is rejected. The hexagonal + square model gives a good fit for both vernier discrimination observers while all other models are rejected. The fit to the hexagonal + square model is shown in Fig 8 and Fig 9 (dark lines through the data).

The decomposition of the total orientation dependence into hexagonal and square components is shown in Fig 10. The middle plot in each of the four parts

- - - - - - - - - -

FIG 10

- - - - - - - - - -

shows the fit to the hexagonal + square model along with the data from Fig 8 and Fig 9 with the mean value subtracted. Immediately above and below each fit is separately plotted the hexagonal and square component respectively. There are a number of noteworthy features. First, the phases of the hexagonal components are fairly closely aligned across tasks and across observers, having a minimum near 90°. While this orientation represents a vertical vernier target, the corresponding grating is horizontal. This is an important observation since it demonstrates that the orientation on which the hexagonal component primarily depends is not the orientation along which the jnd is being measured (the jnd's are measured along orthogonal directions for vertical vernier targets and horizontal gratings) but some other direction, and a possible explanation is given below. The square component for the vernier data also has a minimum near 90° (and 0°). The square components for the spatial frequency data (which are only marginally statistically significant) seem to be more octagonal (period = 45°) than square.

The results above show that a model consisting of the sum of a hexagonal plus a square component, each with even symmetry, is sufficient to explain the observed orientation functions reported here, and both components are necessary within this model. The necessity of the hexagonal and square components can also be established in a very strong model independent manner, leading to the conclusion that it is essentially impossible for any model which lacks either component to fit the data.

DISCUSSION

These results demonstrate that the hyperacuity thresholds reported here display an orientation anisotropy having components with both hexagonal and square symmetry. This effect cannot be an artifact since our display apparatus was circularly symmetric. Although a square component or 'oblique effect' is most often reported in spatial tasks as a function of orientation[16-19], Caelli _et al_. have recently reported spatial frequency discrimination data that also clearly show a strong 60° periodicity for one observer and what appears to be a mixture of 60° and 90° components for other observers.[20] Since in our study, two quite different tasks, spatial frequency discrimination and vernier offset discrimination, both show a hexagonal component we conclude the underlying cause must be general. Extending arguments made previously, we attribute the hexagonal orientation anisotropy of hyperacuity to the existence of a cortical representation of an image, which we refer to as a neural lattice, that preserves the hexagonal symmetry of the retinal photoreceptor lattice. We present below a specific model to explain the manifestation of the hexagonal symmetry in tasks involving the measurement of spatial separations. This model does not account for all orientation effects in spatial vision and in particular the origin of the square component is not addressed.

The Hexagonal Component

The basic proposal we make for the hexagonal component is quite simple: the human visual system does not measure separations or distances in arbitrary directions. Rather there exist a set of intrinsic directions fixed by the orientation of the observer's head and the hexagonal structure of the photoreceptor lattice, and distance is assumed to be measured parallel to one of these directions. As a consequence the 'effective' distance between two parallel lines is not necessarily the perpendicular distance but rather the distance measured along one of the intrinsic directions, presumably the one closest to the perpendicular. The usual identification of the perpendicular distance as the 'true' or objective distance rests on the unstated assumption that the visual system possesses rulers at every possible orientation. However the hexagonal symmetry reported here suggests that there are only three such intrinsic measurement directions, separated by 60°, presumably due to a cortical reflection of the hexagonal photoreceptor packing.

More specifically, we have previously argued that the human visual system measures distances (and spatial frequencies) by identifying features on a neural lattice (for instance, two successive peaks in the case of a sinewave grating or perhaps points of inflection[21], the exact feature being irrelevant here) and then counting the number of lattice points separating them. We make here the additional suggestion that this counting can only be done along the basis directions of the lattice, the directions for which the lattice is most closely spaced. The net result is an enormous reduction in the complexity of the distance measuring mechanism since it need not deal with arbitrary directions, but at the price of potentially introducing orientation-dependent errors in distance measurements. If the perpendicular distance between two lines is s_p, the 'effective' distance measured along one of the intrinsic lattice directions is $s_p/\cos(A)$ where A is the angle between the perpendicular and the nearest lattice direction. Since the intrinsic lattice directions are separated by 60°, A cannot exceed 30° and the maximum effect is an effective distance $s_e = s_p/\cos(30°) = 1.15\ s_p$, a $\pm$ 7.5% effect. The typical error introduced by this mechanism is given by the standard deviation of cos(A) between $\pm$ 30° which is 4%. The smallness of the effect is due to the flatness of the cosine function over a considerable region around zero. Since spatial frequencies are proportional to 1/s the effective spatial frequency f_e will be $f_e = f_p \cos(A)$ where f_p is the frequency measured perpendicular to the wavefronts. Note that effective distances are always larger and the effective spatial frequencies are always lower than the corresponding perpendicular measurements. (The above arguments assume perpendicular projections onto the lattice directions. The projections might instead involve some sort of dogleg along the lattice directions, modifying the above formulas somewhat. The magnitude of the effect is unchanged and effective distances are again always larger, but the exact relationship becomes

$$s_e = s_p * \cos(30°-A)/\cos(30°).)$$

- - - - - - - - - - -

FIG 11

- - - - - - - - - - -

Since the expected hexagonal orientation effects derived above are fairly small, it follows that they would be difficult to observe directly. However, we have previously shown that at certain transition frequencies spatial frequency discrimination is a very rapidly changing function of frequency, and this can be used to amplify the effect. Fig 11 shows $\Delta f_p/f_p$ as a function of the reference frequency f_p for gratings at 0° orientation (vertical) for observer SC. We have previously shown that this function consists of segments which are straight lines passing through the origin (drawn in the figure) separated by transition regions (the first at ~ 4 c/deg) where $\Delta f_p/f_p$ falls rapidly with frequency.[1] Given the arguments above, we should have plotted $\Delta f_e/f_e$ as a function of f_e where f_e is the effective frequency as measured by the observer. Since $\Delta f_e/f_e = \Delta f_p/f_p$ the y axis is unchanged but all values on the x axis should actually be replaced by $f_p \cos(A-A_e)$ where A is 0° for all points on the graph and A_e is the closest intrinsic measurement direction. For simplicity assume A_e is 0° and the x axis is actually f_e. Suppose we tested observer SC at a nominal frequency of 4.0 c/deg and an orientation of 0°. Then we should get the value of $\Delta f/f$ shown in Fig 11 (~ .016). Now suppose we changed the grating orientation by 30° while keeping the perpendicular frequency fixed. This reduces the effective frequency to 4.0 * cos(30°) = 3.5 cycles/deg and we should now measure $\Delta f/f$ ~ .028. In effect changing the orientation by 30° causes the effective frequency to walk along the x axis in Fig 4 from 4.0 to 3.5 cycles per degree, and $\Delta f/f$ should vary by the corresponding amount on the y axis. Increasing A to 60° causes f_e to walk back to 4.0 cycles/deg. Inspecting Fig 1a and allowing for the fact that A_e was not actually 0° indicates that this is nearly the case, with the orientation data oscillating roughly between the limits expected from Fig 11. The orientation data was somewhat lower than expected, perhaps partially due to some contribution from the square component or to a small practice effect. Note also that the nonlinearity in the frequency discrimination function near the transition will lead to a potentially complicated shape for the hexagonal component even though the effective frequency is a fairly simple function of orientation. Actually the fitted hexagonal components (Fig 3) have relatively narrow dips and fairly flat maxima, possibly indicating that the effective frequency walked to the top of the transition in Fig 4 and then started moving down the first segment. The results for JH are similar with the transition occuring at a somewhat higher frequency. Notice that we have exploited the transition region in Fig 11, where $\Delta f/f$ is a rapidly changing function of f, in order to magnify the expected small effects of orientation and produce the striking results of Fig 1. At higher frequencies the transitions are smaller and we expect the hexagonal component to be much smaller. The exact shape of the hexagonal component for the two tasks is almost identical for observer SC but not for JH. However we do not feel that there is any reason to expect that the shape should be exactly the same for the two tasks since we expect that it depends quite critically on aligning the transitions for the two tasks (shown in Fig 11 for frequency discrimination and discussed below for vernier discrimination). Indeed we expect the shape of the component to vary quite strongly for both tasks as the spatial frequency or gap size is varied due to the severe nonlinearity of the frequency discrimination function near the transition regions.

Arguments identical to the ones above can be used to explain the hexagonal component in the variation of vernier discrimination as a function of line segment orientation. Vernier offset thresholds have been shown to be a function of the length of the gap between the two lines.[22] The effective length of this gap will vary with orientation similarly to the effective period of the grating, and if

the vernier threshold vs gap size function shows transitions comparable to those in spatial frequency discrimination the expected small hexagonal component will be magnified. Further, this explains why the hexagonal component has a minimum for vertical vernier targets and horizontal spatial frequency gratings. As can be seen in Fig 10 the hexagonal components of the two tasks are in phase when the gap of the vernier stimulus is perpendicular to the bars of the grating and thus aligned with the direction between bars along which spatial frequency is measured. This is consistent with our expectation that the variable which primarily determines the hyperacuity threshold (the scale setting variable) is the gap for a vernier target and the distance between bars for a grating. Note also that the two observers are nearly in phase with respect to the hexagonal component. If, as we propose, the hexagonal component is fundamentally attributable to the photoreceptor lattice, this suggests that the photoreceptor lattice has a fixed orientation and very likely has the same orientation in both eyes.

The Square Component

The square component observed in the vernier discrimination data is presumably related to the commonly reported 'oblique effect'. Although the origin of the square component is not discussed in this paper we assume it is distinct from the hexagonal component with which we are primarily concerned here. It should be noted that the square component shows far less task to task consistency in our data than the hexagonal component, possibly indicating a less fundamental origin.

CONCLUSION

Guided by an extension of our previously reported model of spatial-frequency discrimination, we have shown that hyperacuity thresholds as a function of stimulus orientation contain a component with hexagonal symmetry. We assume that this hexagonal symmetry is fundamentally related to the hexagonal packing of photoreceptors. Since the magnitudes of similar hyperacuity thresholds have previously been related to the center-to-center spacing of photoreceptors[1], we conclude that there is now strong evidence for the role of the photoreceptor lattice in spatial vision. In addition, at least some spatial tasks have a component with square symmetry in their orientation dependence. We propose a model of spatial vision in which the photoreceptor lattice provides the only geometrical element, with all other elements being topological.

4. SPATIAL FREQUENCY DISCRIMINATION FOR LOW SPATIAL FREQUENCIES.

In a recent paper we reported that the ability of human observers to discriminate between different spatial frequencies was not a smooth function of frequency but rather had a definite segmented structure.[9] We interpreted this structure as being due to reconstruction of the images on a set of cortical lattices with discrete effective spacings of ε/N where ε was found to be the foveal photoreceptor spacing ($\sim$ 0.008 deg) and N was an integer factor attributable to cortical interpolation. However these previous results were restricted to spatial frequencies above 2 cycles/degree (c/deg) and our model did not deal with lower frequencies. In this study we extend our measurements to frequencies as low as 0.3 c/deg and the model to all visually accessible spatial frequencies. For spatial frequencies between 0.3 and 2 c/deg we find a very similar ε/N segment structure

with ε equal to about 0.056 deg or 7 times the foveal photoreceptor spacing. We attribute this to spatial sampling by an array of retinal receptive fields which we call spatial sampling fields and which also perform a neural blurring analogous to the blurring of high frequencies by the optics of the eye.

METHODS

The methods used are identical to those previously described except that the gratings consisted of narrow bright lines on a dark background rather than suprathreshold sinusoidal gratings. Briefly, each experimental session employed a fixed reference frequency and either 7 or 9 test frequencies chosen symmetrically around the reference frequency. Each trial consisted of the presentations of a reference grating for 0.75 sec, an interstimulus interval of 0.75 sec, and a test grating for 0.75 sec. The observer responded by indicating whether the test grating had a higher or lower spatial frequency than the reference. Following each response a synthesized voice indicated the correct choice. The test and reference phases were independently randomized on each trial and test frequencies were randomized together according to the method of constant stimuli. There were usually 50 trials per test stimulus and at least 40. Distance from the observer to the display, a Tektronix 606 monitor, was varied so that there were always at least 3 lines on the screen. Head stabilization was achieved by adjustable chin and forehead rests with snug cushions on both sides of the head. Viewing was central but with no explicit fixation target. The data from each session were fit to a cumulative normal distribution to determine the just noticeable difference (jnd) in frequency Δf, defined as the change in frequency necessary to raise the probability of a correct response from 0.5 to 0.75. The fitting procedure also provided an estimate of the statistical error in Δf for each session. Following our previous work, we consider the separation between bars $s = 1/f$ as the critical stimulus, not f. However in what follows we will generally use f and s interchangeably. Further, we have shown that $\Delta s/s = \Delta f/f$, and note that the inverse of separation is dimensionally the same as spatial frequency.

RESULTS

Fig. 12 shows the results of this experiment for four observers: GC, CS, SC

- - - - - - - - - - -

FIG 12

- - - - - - - - - - -

and SG. The fractional jnd in spatial separation $\Delta s/s$ is plotted against the inverse of spatial separation s where $s = 1/f$ is the distance between lines in the grating. The data are clearly not smooth functions of frequency but cluster around straight lines drawn through the origin, with transitions between the line segments occurring regularly at about every 0.6 ~ 0.7 c/deg. This segmented structure has been seen previously at higher spatial frequencies (above 2 c/deg) where the spacing between transitions was about 4 c/deg.

Fig. 13 shows the high frequency Δf/f function for a fifth observer, JH.

- - - - - - - - - - -
FIG 13
- - - - - - - - - - -

(The data on this figure below 16 c/deg have previously been published). Note that the segmentation and the average value of Δf/f are quite similar to that in Fig. 12. For these high frequencies it was found that the slopes of the line segments took on the values ε/N where ε was about 0.008 deg (the center to center spacing of foveal photoreceptors) and N was an integer.

We have fit the data in Fig. 12 to a similar ε/N form. Excluding the few points which clearly fall in transition regions and a few aberrant points which are not consistent with their neighbors gives acceptable fits to this model (chi squared confidence level >10%). As was also found in the previous high frequency experiments, the transition frequencies at which the function jumps from one line segment to the next are not quite evenly spaced for reasons that are not understood. Nevertheless the overall agreement between the data and model is fairly good. The best fit values of ε for the four observers are: 0.054 ± 0.001 (CS), 0.055 ± 0.001 (SC), 0.059 ± 0.001 (SG) and 0.030 ± 0.0005 deg (SG). There is good agreement for all but the last observer, SG. However, this atypical observer also has the lowest value of ε for the high-frequency band (> 2 c/deg) that we have encountered so far (ε = 0.0056 deg where 0.008 is typical) and is not included in the average.

DISCUSSION

The discussion here closely parallels the earlier discussion of the high frequency results. As shown in our previous work a straight line passing through the origin in the Δf/f vs f plane is a region in which the jnd in spatial interval Δs is constant. Thus the segments of slope ε/N are regions in which there is a constant spatial jnd Δs = ε/N. Following our previous work we attribute each segment to the existence of a cortical lattice with effective spacing ε/N. For N = 1 the cortical lattice has the same effective spacing as the retinal spatial sampling lattice while the higher N lattices are constructed by interpolating between the retinal samples onto a cortical lattice with a spacing N times finer than the spacing of the retinal lattice. This scheme represents a highly efficient use of the retina to cortex connections. For the high frequency band (above 2 c/deg) the fundamental spacing ε was found to be about 0.008 deg or one photoreceptor, and as seen from Fig. 13, N may be as high as 8 (taking ~32 c/deg as the high frequency limit), although it would be very difficult to prove that all the intermediate values of N exist. For the frequency band from 0.3 to 2 c/deg (which we call the mid-frequency band), ε is about 0.056 deg or 7 times the spacing of the photoreceptor and N goes from 1 to 4. We attribute this value of ε to the existence of a class of retinal receptive fields, the mid-frequency spatial sampling fields, which have a center to center spacing of 0.056 deg. These fields have two functions. First, they perform a spatial sampling function analogous to that of the photoreceptor, reducing a continuous luminance distribution to a finite number of measurements per unit interval for transmission to the cortex, but on a larger scale and thus drastically reducing the number of fibers required in the optic nerve. However, cortical interpolation between samples is impossible unless

the image is sufficiently blurred to excite at least three sample points (in one dimension).[1,2,3] For the high spatial frequencies this blurring is performed by the optics of the eye.[24] For the mid-frequency band the blurring must be accomplished neurally by overlapping the spatial sampling fields to a considerable extent. Thus the widths of the fields must be several times their center-to-center separation or about 0.1 ~ 0.2 deg full width at half maximum for the excitatory center.[25] This is in reasonable agreement with previous psychophysical estimates of receptor field sizes. For example, Wilson and Gelb propose a model having a discrete set of 6 receptive field sizes of which one has a center spacing of 0.055 deg (with a 0.25 octave observer to observer variation) and another has a center spacing of 0.047 deg, both quite comparable to the values reported here.[26] The receptive field widths estimated by Wilson and Gelb are also comparable to our somewhat poorly constrained estimates.

Scaling

One of the remarkable features of Figures 1 and 2 is that the average value of $\Delta f/f$ or $\Delta s/s$ is fairly constant over a rather large range of frequencies. We attribute this to a scaling property of the visual system in which the cortical lattice on which an image is analyzed is always chosen such that $\varepsilon(s)/s$ is roughly constant where $\varepsilon(s)$ is the lattice spacing and s is the characteristic size or spatial scale of the feature being analyzed. (For a grating s is the distance between bars.) Since $\varepsilon(s)$ will clearly be related to the spatial resolution, the net effect is that resolution scales with image size so that the fractional resolution appears roughly constant.

Consider how many cortical maps are required for such a scaling system. From Fig. 13 it is clear that 8 maps suffice to cover spatial scales from 1/32 to 1/2 deg, which we label the high frequency band. From Fig. 12 we can see that 4 maps are sufficient to cover spatial scales from 1/2 to 3.5 deg, the mid frequency band. We will assume that Fig. 13 repeats two more times for still lower frequencies with the spatial scale increasing each time by a factor of 7. That is, we assume that there exist two more classes of retinal sampling fields, one with center-to-center separation of 0.4 deg and one with center-to-center spacing of 2.8 deg. The former would mediate the low frequency band (spatial scale 3.5 deg to 25 deg) and the latter the very low frequency band (25 deg to 175 deg). Each of these bands is assumed to be subdivided into 4 segments by the cortical interpolation mechanisms. Thus a total of 20 cortical lattices would suffice to cover all scales accessible to the human visual system, a 5600:1 range, while keeping $\Delta s/s$ constant to within 2:1 in the worst case (the N=1 to N=2 transition). The typical deviation is much smaller with the rms deviation being about 16% of the mean. The well established rise in resolution with eccentricity[27-30] presumably occurs because progressively finer maps are restricted to progressively smaller eccentricities.

Note that the notion of scaling presented here differs quite fundamentally from the usual concept of cortical magnification.[31-34] The conventional model assumes the existence of a single nonlinear mapping between retina and cortex, which can be pictured as a set of narrow concentric annuli of increasing inverse cortical magnification resulting in a continuous local scaling with eccentricity. This is not consistent with the finding presented here that coarse spatial quantization also exists in the central retina, although one could add coarser maps

with similar continuous nonlinear scaling properties. We propose instead (or perhaps in addition) the existence of a set of about 20 linear maps with automatic scale selection to achieve an apparent scale independence. This can be pictured as a set of overlapping concentric disks of differing but constant cortical magnification, with the coarser maps extending to greater eccentricities. If we assume the total extent of a map to be proportional to the lattice spacing (i.e., the number of points in each map constant), the apparent inverse cortical magnification factor will be roughly proportional to eccentricity, where the apparent magnification is presumed to be due to the finest map at the given eccentricity. The scaling in this model is primarily with feature size, with the eccentricity scaling being somewhat incidental, and also not continuous.

Linear maps offer great advantages over nonlinear maps. In particular, it is generally quite difficult to measure distance on a nonlinear map, since this requires integrating variable magnification factors over some hard to specify path. Further, an image which extends over a region in which the nonlinear magnification factor varies significantly will generally be subject to large position-dependent distortions, greatly complicating pattern recognition, although some non-linear mappings may have useful properties.[35] The mechanism we propose avoids these problems while still achieving apparent scale invariance.

CONCLUSION

We have shown that spatial frequency discrimination as a function of frequency in not a smooth function of frequency for frequencies between 0.3 and 2 c/deg but rather has a segmented structure similar to that observed for spatial frequencies above 2 c/deg. We interpret this as evidence for spatial quantization by retinal spatial sampling fields having a center-to-center spacing of about 0.056 deg. We suggest that there may also exist spatial sampling fields with center-to-center spacing of 0.4 deg and 2.8 deg. We propose a scaled lattice model of spatial vision which allows apparently scale independent spatial processing while retaining the benefits of linear maps.

5. A MODEL OF SPATIAL DISCRIMINATION

THE SCALED LATTICE MODEL OF SPATIAL VISION

We present here an outline of the scaled lattice model of spatial vision. The reader must be cautioned that the development of the model is in an early stage and there are major aspects which need to be further addressed experimentally. Notably, we neglect binocular vision, two dimensional considerations, temporal effects, and the interaction between multiple simultaneously present spatial scales. However the following provides a listing of some important elements and a basis for future development.

1. Retinal images are optically blurred and sampled by photoreceptors. In the central region of the retina the output of each photoreceptor (perhaps after convolution with some local weighting function designed to remove low frequencies) is then transmitted to the cortex for further processing. Over the central and larger regions photoreceptors are pooled into regularly spaced spatial sampling fields with overlapping excitation functions designed to remove high frequencies

and provide sufficient neural blurring to allow interpolation between field centers. Only one output per spatial sampling field is transmitted to the cortex. There are presumably a sequence of classes of spatial sampling fields of increasing center-to-center spacing with the spatial extent covered by each class presumed proportional to the spacing of that class. That is, the optic nerve per each photoreceptor sampling and all the classes of receptive field sampling coexist in the central part of the retina but the coarser samplings extend to greater eccentricities. The point of this scheme is to efficiently encode the position information in the retinal image by sampling near the sampling limit for multiple spatial scales and thus minimize the number of cortical connections. The multiple scales of sampling allow more detail to be encoded at smaller eccentricities.

2. The image is reconstructed in the cortex for a given sampling scale by interpolating between sample points onto a neural lattice whose spacing is an integer (N) times finer than the sample spacing. Note that there is no information in this reconstruction that was not present in the original sampling. The neural lattices (with $N > 1$) basically represent an unpacking of the highly encoded information in the original sampling into a form in which the position information is more accessible, with higher values of N allowing more detailed unpacking and hence more accurate localization of the features of the image. The interpolation may include convolution with a function designed to enhance some aspect of the image or to remove frequencies too low to be of interest. The total spatial extent of each lattice is assumed proportional to the effective lattice spacing, resulting in an apparent inverse cortical magnification factor that is a roughly linear function of eccentricity.

3. The positions of local features such as peaks or perhaps points of inflection[36] are determined to the nearest lattice point by comparing neighboring points in the neural lattice. For example, peaks can be localized by testing three successive points to see if the sign of the slope has changed.

4. Spatial intervals are measured by counting points in the neural lattice between the features located above. Assuming the localization procedure is sufficiently accurate, the error (jnd) in the spatial interval will then be dominated by the effective spacing of the neural grid. Thus the neural lattices, which are derived from the photoreceptor lattice, serve as rulers of differing scales for the measurement of spatial intervals.[37,38]

5. There exists an automatic scale selection mechanism which chooses the sampling scale and interpolation factor such that the effective lattice spacing is roughly proportional to the spatial scale of the measurement. Thus $\Delta s/s$ is roughly constant, where Δs is the spatial resolution and s is the spatial scale. The motivation of this scaling is to keep the total number of elements required at a tractable number independent of the image size.

- - - - - - - - - - -

FIG 14

- - - - - - - - - - -

Fig 14 is an illustration of the scaled lattice model. For clarity we show only the fundamental photoreceptor sampling and a 3:1 interpolation. Part a) shows the external luminance distribution, a delta function. Part b) shows the luminance distribution after blurring, and c) shows the sampling of the image by the

photoreceptors. Part d) represents the interpolation process, which accepts the coarsely sampled input from the photoreceptors and produces a more finely spaced sampling on the neural lattice (e). We have drawn the neural unit spacing as 1/3 the photoreceptor spacing, but in general it can be 1/N where N is an integer. Part f) illustrates local feature detection on the neural unit lattice, showing a peak detector (square) receiving input from three adjacent neural units. Part g) is a possible realization of a position independent separation detector using pre-counted intervals for speed. The separation detector performs the function Peak (x) and Peak (x + s) ORed over all x, and would have many properties usually attributed to spatial frequency selective channels with spatial summation.

REFERENCES

1. H.B. Barlow, 'Reconstructing the visual image in space and time', Nature, 279, 189-190 (1979).

2. G. Westheimer, 'The spatial sense of the eye,' Invest. Ophthalmol. Visual Sci, 18(9), 893-912 (1979).

3. M. Fahle, T. Poggio, 'Visual hyperacuity: spatiotemporal interpolation in human vision', Proc. R. Soc. Lond. B, 213, 451-477 (1981).

4. It was found that the contrast matching experiments were necessary for medium and high spatial frequencies because test gratings of different frequencies and equal contrasts had perceptibly different apparent contrasts due to the slope of the modulation transfer function. The contrast matching experiments were similar to the frequency discrimination experiment described here. The reference grating was presented at 30% contrast and one test grating frequency was randomly presented at seven different contrast levels. On each trial the observer indicated whether the contrast of the test grating was higher or lower than the contrast of the reference grating. A contrast level that appeared equivalent to the reference grating at 30% contrast was determined from the psychometric function.

5. G. Westheimer and S.P. McKee, 'Spatial configurations for visual hyperacuity', Vision Res., 17, 941-947 (1977).

6. G. Westheimer and S.P. McKee, 'Integration regions for visual hyperacuity', Vision Res, 17, 89-93 (1977).

6. Williams, D.R. and Collier, R. (1983). Consequences of spatial sampling by a human photoreceptor mosaic. Science, 221, 385-387.

7. Miller, W.H. and Bernard, G. (1983). Averaging over the foveal receptor aperture curtails aliasing. Vision Res. (in press).

8. Yellott, John I. Jr., (1982). Spectral analysis of spatial sampling by photoreceptors: Topological disorder prevents aliasing. Vision Res., 22, 1205-1210.

9. Hirsch, J. and Hylton, R. (1982). Limits of spatial frequency discrimination as evidence of neural interpolation. J. Opt. Soc. Am. 72, 1367-1374.

10. Miller, W.H. (1979). Handbook of Sensory Physiology, VII(6A), Fig. 30, p.118, Springer Berlin.

11. Borwein, B., Borwein, D., Medeiros, J. and McGowan, J. W. (1980). The ultrastructure of monkey foveal photoreceptors, with special reference to the structure, shape, size and spacing of the foveal cones. Am. J. of Anatomy, 159, 125-146.

12. Polyak, S.L. (1957). The Vertebrate Visual System. University of Chicago Press, Chicago., Fig. 156.

13. Kittel, C. (1971). Introduction to Solid State Physics (4th ed). John Wiley and Sons, Inc., New York.

14. Bowker (1979) studied the orientation dependence of spatial frequency discrimination at several reference frequencies including 4 c/deg. He reported no evidence for orientation dependence at this frequency. There are two possible explanations for the discrepancy between those observations and the observations reported here. First, we find that the choice of reference frequency is fairly critical as discussed in more detail later. Second, in the Bowker study, the orientation function was only sampled at 45° intervals, which is below the sampling limit for all harmonics of the hexagonal component and also for all but the fundamental of the square component. Indeed, aliasing of these higher frequency components is a potentially serious problem with such a coarse sampling.

Bowker, Duane O. (1980) Spatial frequency discrimination thresholds in different orientations. J. Opt. Soc. Am. 70/4, 462-463.

15. McKee, S.P. and Westheimer, G. (1978) have reported that the effects of orientation on vernier acuity decreased substantially after practice. To avoid practice effects observer SC completed over 8,000 trials of preliminary data before the final data reported here were collected, and JH, an extremely experienced observer, completed at least 4,000 initial trials. Although the effects of large numbers of repetitions was not studied here, the essential results were replicable over the three month period of data collection. A possible explanation for the 'practice effect' may be subtle head movements empolyed by the observer to improve performance on non-preferred stimulus orientations. We encountered such a problem and solved it by improving head stabilization. This is an interesting point in that it indicates that observers may be to some degree aware of the existence of optimal orientations and attempt to tilt their heads to exploit them.

McKee, S.P. and Westheimer,G. (1978) Practice effects of orientation. Perception and Psychophysics 24, 258-262.

16. Mitchell, D.E., Freeman, R.D. and Westheimer, G. (1967) Effect of orientation on the modulation sensitivity for interference fringes on the retina. J. Opt. Soc. of Am., 57, 246-259.

17. Matin, E. and Drivas, A. (1979) Acuity for orientation measured with a sequential recognition task and signal detection methods. Perception and Psychophysics, 25, 161-168.

18. Tyler, C.W. (1977) Orientation differences for perception of sinusoidal line stimuli. Vision Res. 17, 83-88.

19. Appelle, S. (1972) Perception and discrimination as a function of stimulus orientation: The 'oblique effect' in man and animals. Psychol. Bull. 78, 266-278.

20. Caelli, T., Brettel, H., Rentschler, I. and Hilz, R. (1983) Discrimination thresholds in the two-dimensional spatial frequency domain. Vision Res. 23, 129-133.

The most detailed Caelli et al. data is presented in a two-dimensional form that is difficult to compare to the data presented here. However they display summary graphs showing spatial frequency discrimination as a function of orientation averaged over 4, 8, and 12 c/deg which are coincidentally the nominal frequencies at which we expect transitions to occur. For one of their observers (RH, Fig 2d) this function displays an almost pure 60° periodicity although it lacks the even symmetry that we expect, perhaps due to averaging over several transitions. The data for the other two observers (TMC and IR, Figs 1d and 2d) are less clear but appear to be a mixture of hexagonal and square components as is reported here.

21. Watt, R.J. and Morgan, M.J. (1983) Mechanisms responsible for the assessment of visual location: Theory and evidence. Vision Res. 23, 97-109.

22. Westheimer, G. and McKee, S. (1977) Spatial configurations for visual hyperacuity. Vision Res. 17, 941-947.

23. G. Westheimer. Diffraction theory and visual hyperacuity. Am. J. Optom. and Physiol. Optics, 53, 362-364 (1976).

24. F.N. Campbell and D. Green. Optical and retinal factors affecting visual resolution. J. Physiol., 181, 576-593 (1965).

25. Barlow (1964) has previously noted that neural blurring may be an important aspect of receptive field function. Barlow, H.B. (1964) The physical limits of visual discrimination. Photophysiology, Vol. 2. Academic Press. p. 163-202.

26. H. Wilson and D.J. Gelb. A modified line element theory for spatial frequency and width discrimination. J. Opt. Soc. Am. A. In press (1984).

27. G. Westheimer. The spatial grain of the perifoveal visual field. Vision Res., 22, 157-162 (1982).

28. J. Rovamo, V. Virsu, P. Laurinen and L. Hyvarinen. Resolution of gratings oriented along and across meridians in peripheral vision. Invest. Ophthalmol. Vis. Sci., 23, 666-670 (1982).

29. V. Virsu and J. Rovamo. Visual resolution, contrast sensitivity and the cortical magnification factor. Exp. Brain Res., 37, 475-494 (1979).

30. J. Rovamo, V. Virsu, and R. Nasanen. Cortical magnification factor predicts the photopic contrast sensitivity of peripheral vision. Nature, 271, 189-190 (1978).

31. Cortical magnification refers to the extent of striate cortex to which each degree of retina projects (Daniel and Whitteridge, 1961, Cowey and Rolls, 1974).

32. A. Cowey and E.T. Rolls. Human cortical magnification factor and its relation to visual acuity. Exp. Brain Res., 21, 447-454 (1974).

33. P.M. Daniel and D. Whitteridge. The representation of the visual field on the cerebral cortex in monkeys. J. Physiol., 159, 203-221 (1961).

34. J. Rovamo and V. Virsu. An Estimation and application of the human cortical magnification factor. Exp. Brain Res., 37, 495-510 (1979).

35. E.L. Schwartz. Computational anatomy and functional architecture of striate cortex: a spatial mapping approach to perceptual coding. Vision Res. 20, 645-669 (1980).

36. R.J. Watt and M.J. Morgan. Mechanisms responsible for the assessment of visual location: theory and evidence. Vision Res. 23, 97-109 (1983).

37. J. Hirsch and R. Hylton. Quality of the primate photoreceptor lattice and limits of spatial vision. Vision Res., In press (1984).

38. J. Hirsch and R. Hylton. Orientation dependence of hyperacuity contains components with hexagonal symmetry. J. Opt. Soc. Am. A., In press.

FIGURE CAPTIONS

Fig. 1 Fractional jnd in spatial frequency ($\Delta f/f$) as a function of spatial frequency of the reference grating (c/deg) for observers JH, BA and MM. The straight lines passing through the origin represent regions of constant angular jnd Δs. Determination of the lines is discussed in the text.

Fig. 2 Fractional jnd in spatial frequency ($\Delta f/f$) as a function of field size (number of cycles in the reference grating) for observer BA at 4, 8 and 12 cycles/deg.

Fig. 3 Fractional jnd in separation ($\Delta s/s$) as a function of 1/reference separation (deg^{-1}). The straight lines passing through the origin represent the regions of constant angular jnd Δs shown in Fig. 1.

Fig. 4 Comparison of spatial frequency discrimination (4a) and line pair separation discrimination (4b) for observer JH. The data from Figs. 1a and 3 are replotted (Fig. 4a and 4b respectively) to show the similarity between the two experiments as discussed in the text. The dashed lines drawn through the data in both cases are the same as the lines drawn through the origin of Figs. 1 and 3. The data illustrate the step-like characteristic of Δs for both experiments. Open circles show similar line pair separation results previously reported by Westheimer.[2]

Figure 5 Cone inner segments at the central fovea in the retina of the monkey, Macaca fascicularis, shown in a photograph of a 1 μM thick section tangent to and on the sclera side of the external limiting membrane. Center-to-center distance of cones is 3 μM. From Miller (1979) with permission.

Figure 6a Histogram of distances between all pairs of photoreceptors in the sample shown in Fig. 1. The first peak shows the distribution of distances between the centers of nearest neighbors.

Figure 6b Histogram of all angles between the horizontal axis and the lines connecting the center of each photoreceptor to the center of its nearest neighbors. The six peaks demonstrate a high quality hexagonal lattice.

Figure 7 Variance between expected and actual positions of photoreceptors vs. ring number normalized so that the nearest neighbor distance is 1.0. Filled circles correspond to errors in separation (parallel), and open circles correspond to errors in orientation (perpendicular). The curve is a psychophysical estimate of the total parallel variance in spatial interval measurement by humans.

Figure 8 Fractional jnd in spatial frequency, $\Delta f/f$, where Δf is the jnd in frequency and f is the reference frequency, as a function of orientation. 0° represents the vertical (bar) grating orientation. Functions are shown for observer SC for a reference frequency of 4.0 c/deg (1a) and for observer JH for a reference frequency of 4.5 c/deg (1b).

Figure 9 Jnd in offset, Δo, for the vernier offset discrimination task as a function of orientation where 0° represents the horizontal orientation of line segments. Functions are shown for two observers SC and JH with a gap of .25 deg in the vernier target.

Figure 10 The decomposition of orientation dependence into hexagonal and square components for the spatial frequency discrimination task (upper sections) and for the vernier offset discrimination task (lower sections). Center plots in each quadrant show the sum of hexagonal and square components plus the data replotted from Figs 1 and 2 (minus the average). Note that 0° rotation is a vertical spatial frequency grating (top graphs) and a horizontal vernier line segment (bottom graphs).

Figure 11 Fractional jnd in spatial frequency, $\Delta f/f$, as a function of reference frequency for observer SC. The data show a sharp transition between 3.5 and 4 c/deg. This effect has been previously described[1]. The dashed lines illustrate the use of the transition to magnify an anticipated small hexagonal orientation effect as discussed in the text.

Figure 12 Results of the line grating frequency discrimination experiments for spatial frequencies between 0.3 and 2 c/deg. The fractional jnd in separation $\Delta s/s$ is plotted against the inverse of reference separation which is dimensionally equivalent to spatial frequency. Data are shown for four observers: GC, CS, SC and SG. The slopes of the straight lines drawn through the first segments are 0.059, 0.054, 0.055, and 0.030 deg respectively and the family of lines drawn through the data are explained in the text.

Figure 13 Results of the sinusoidal grating frequency discrimination experiment for spatial frequencies between 1.5 and 28 c/deg. The fractional jnd in frequency $\Delta f/f$ is plotted against reference frequency. Data are shown for observer JH, and the slopes of the line segments fit to the data are indicated on the graph. (The region of this graph below 16 c/deg has been published previously.[1])

Figure 14 Schematic of the scaled lattice model. See Apppendix A for discussion.

Joy Hirsch
F49620-83-C-0026

Figure 1

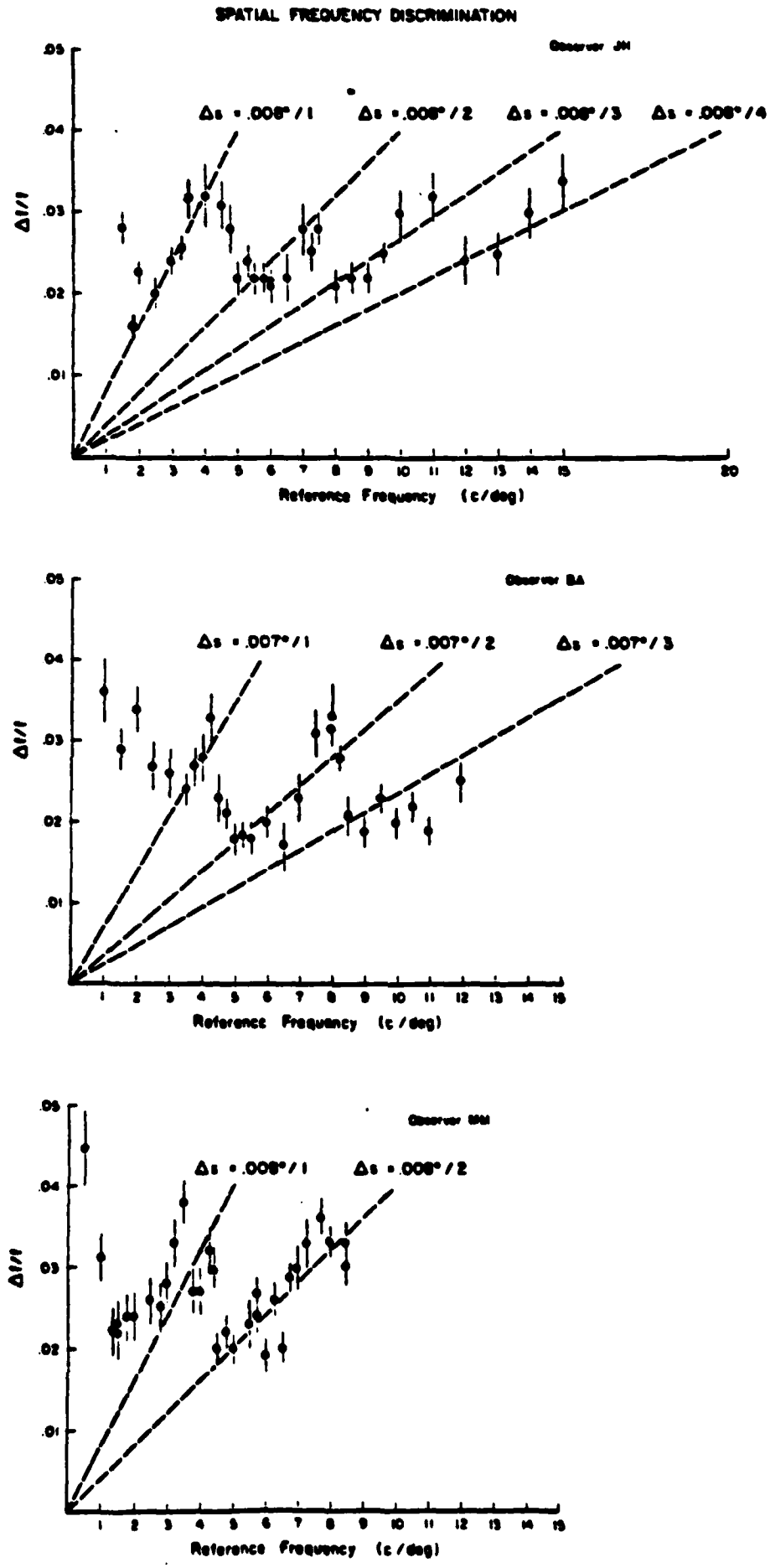

Joy Hirsch
F49620-83-C-0026

Figure 2

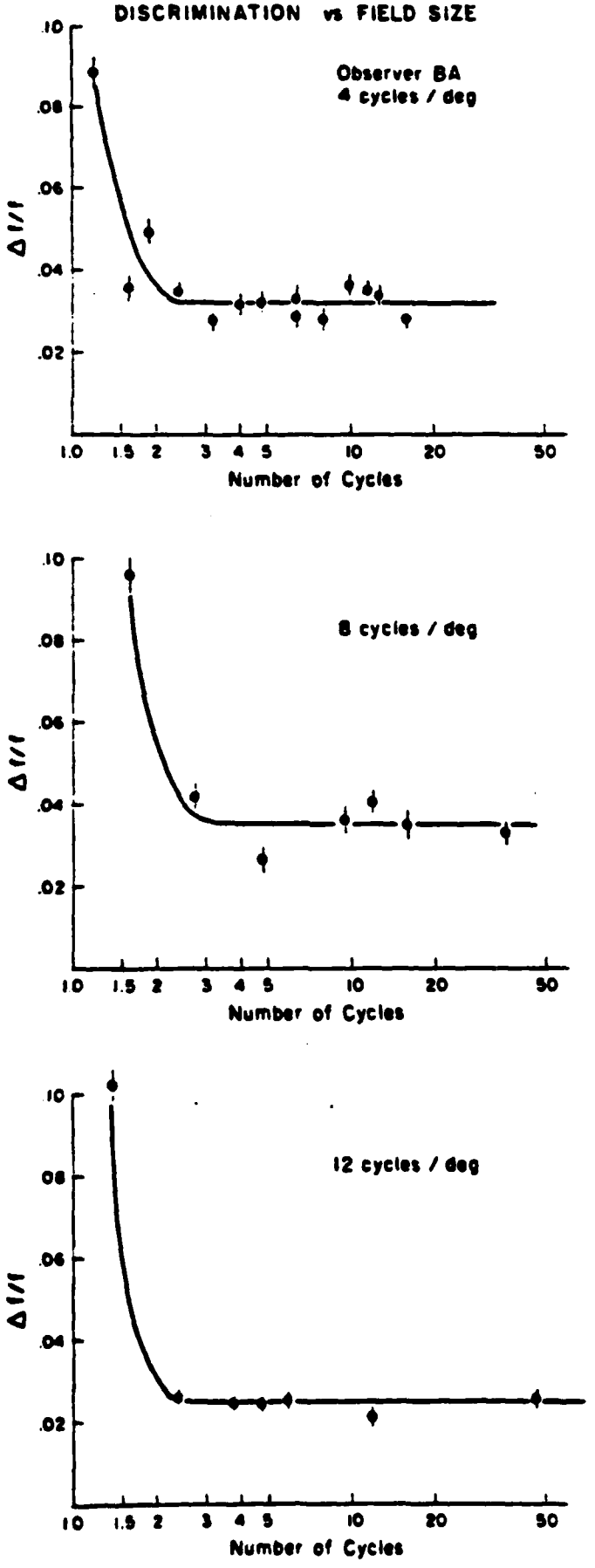

Figure 3

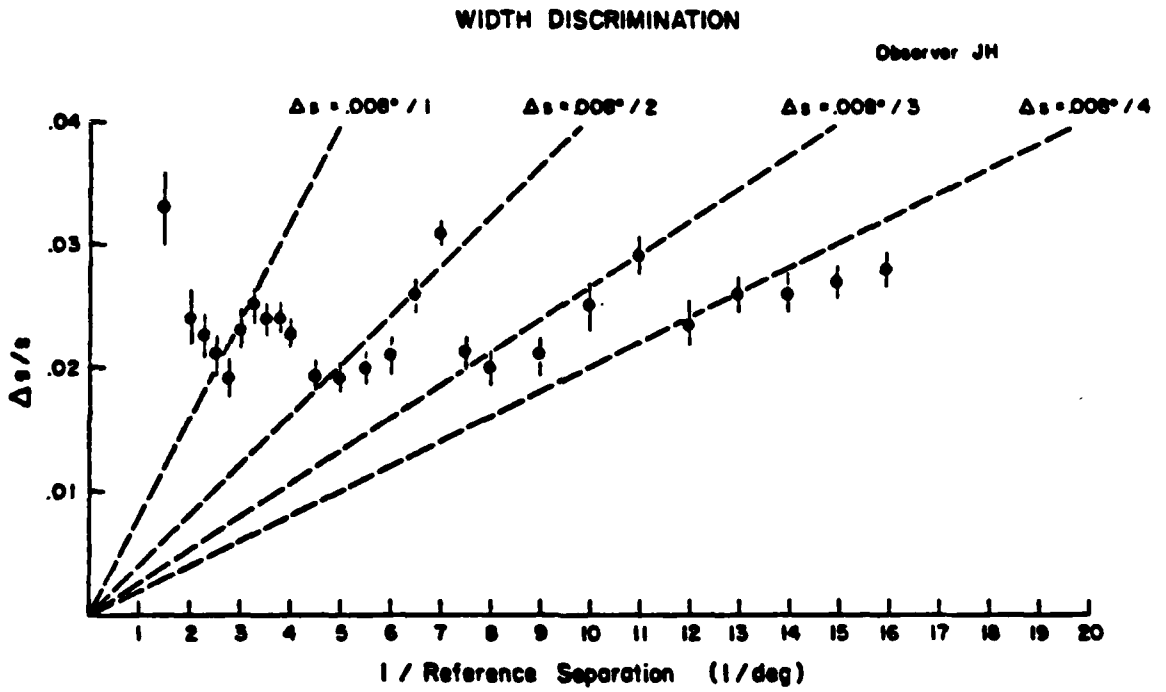
WIDTH DISCRIMINATION
Observer JH
Δs = .008° / 1
Δs = .008° / 2
Δs = .008° / 3
Δs = .008° / 4
.04
.03
.02
.01
Δs/s
1 2 3 4 5 6 7 8 9 10 11 12 13 14 15 16 17 18 19 20
1 / Reference Separation (1/deg)

Joy Hirsch
F49620-83-C-0026

Figure 4

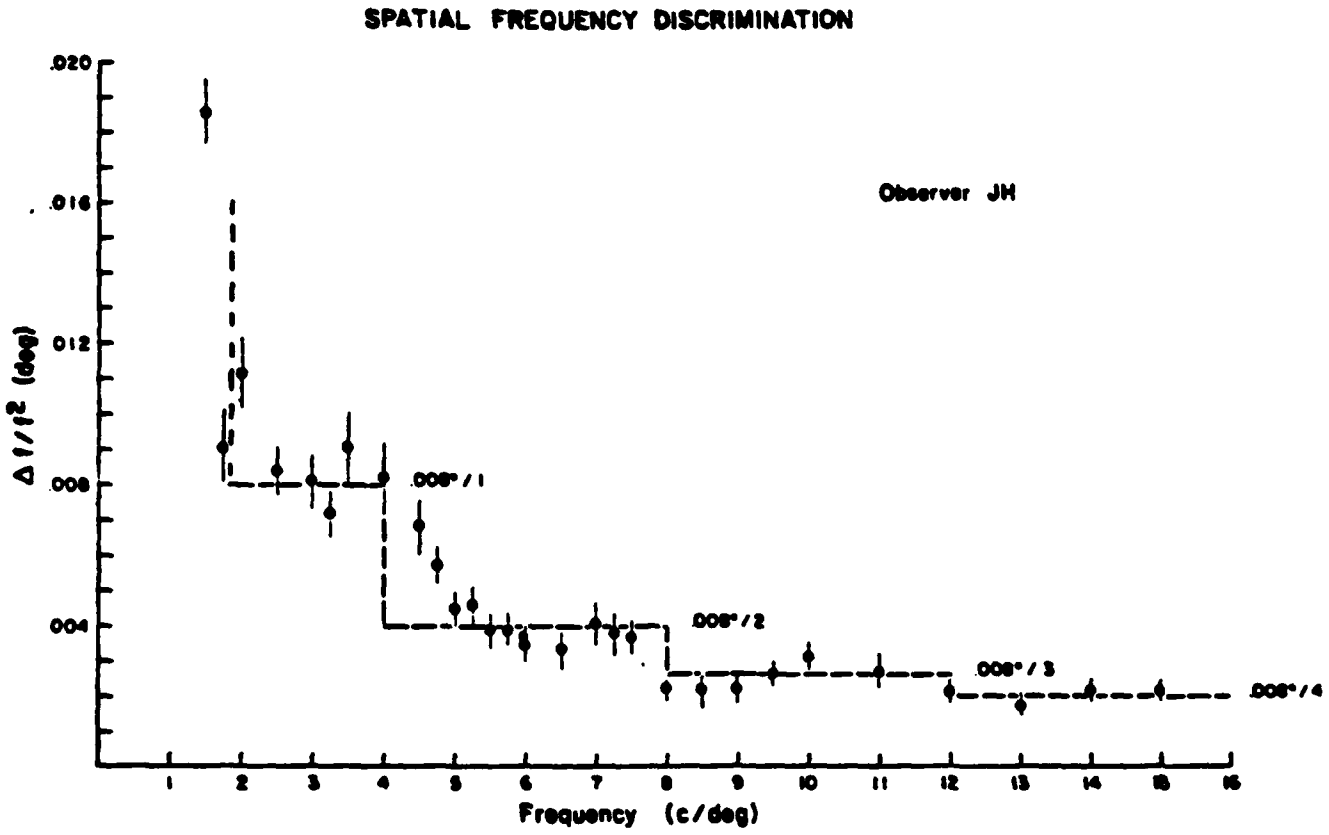

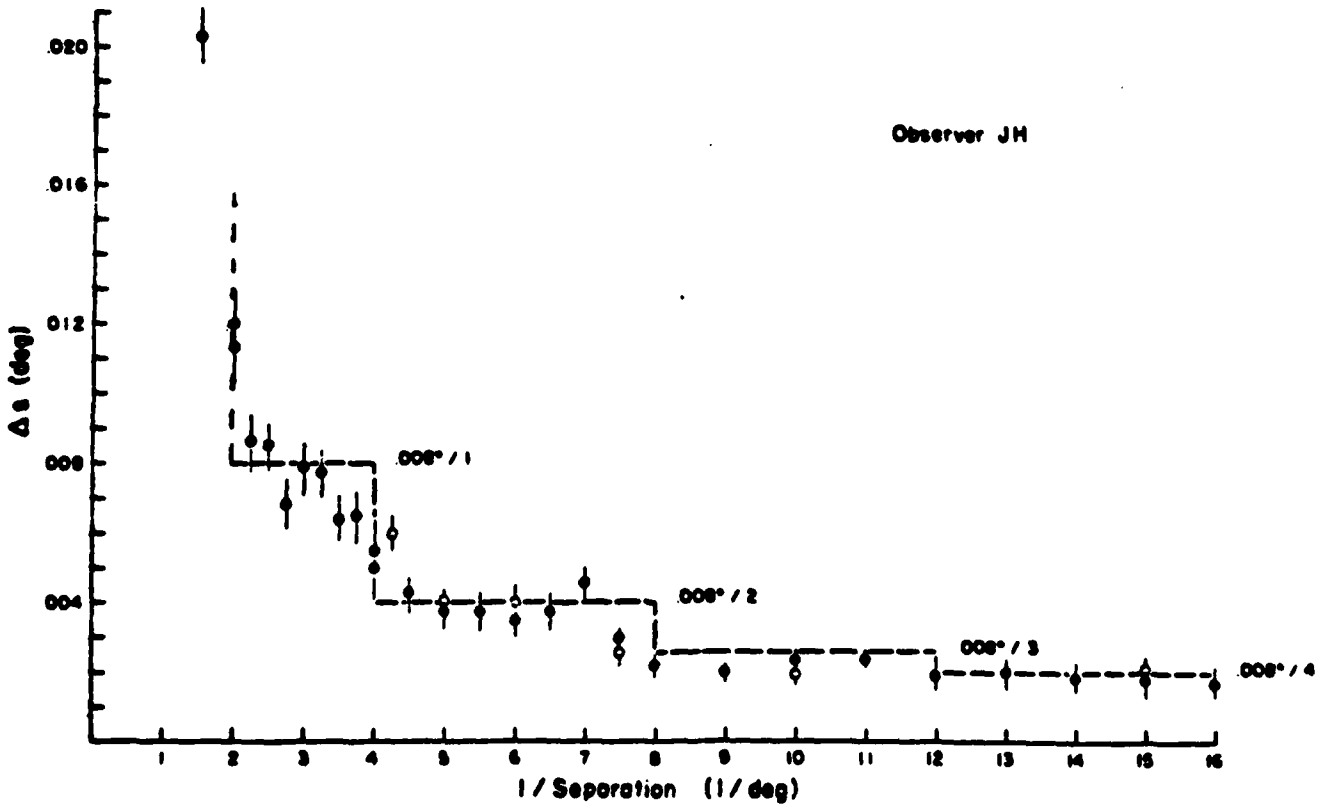

Joy Hirsch
F49620-83-C-0026

Figure 5

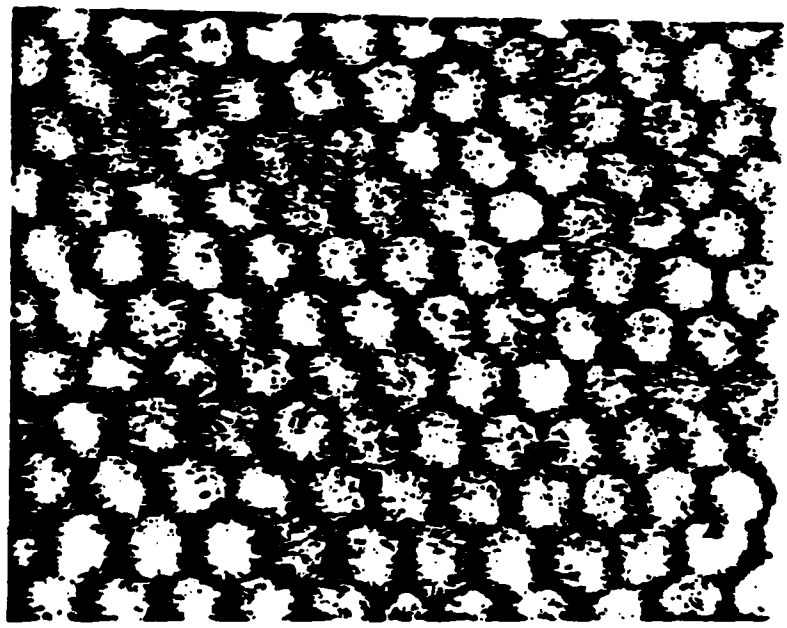

Joy Hirsch
F49620-83-C-0026

Figure 6

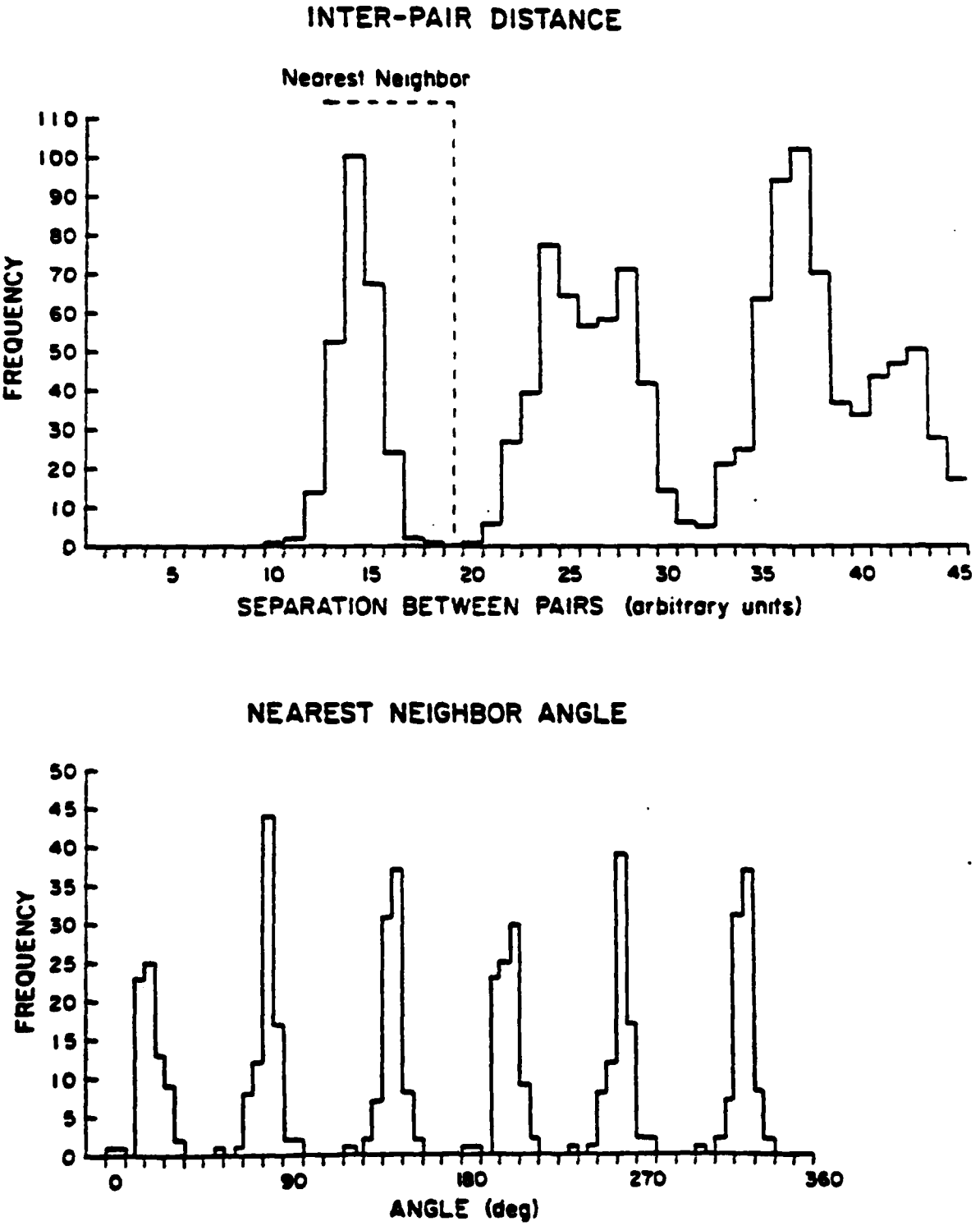

Figure 7

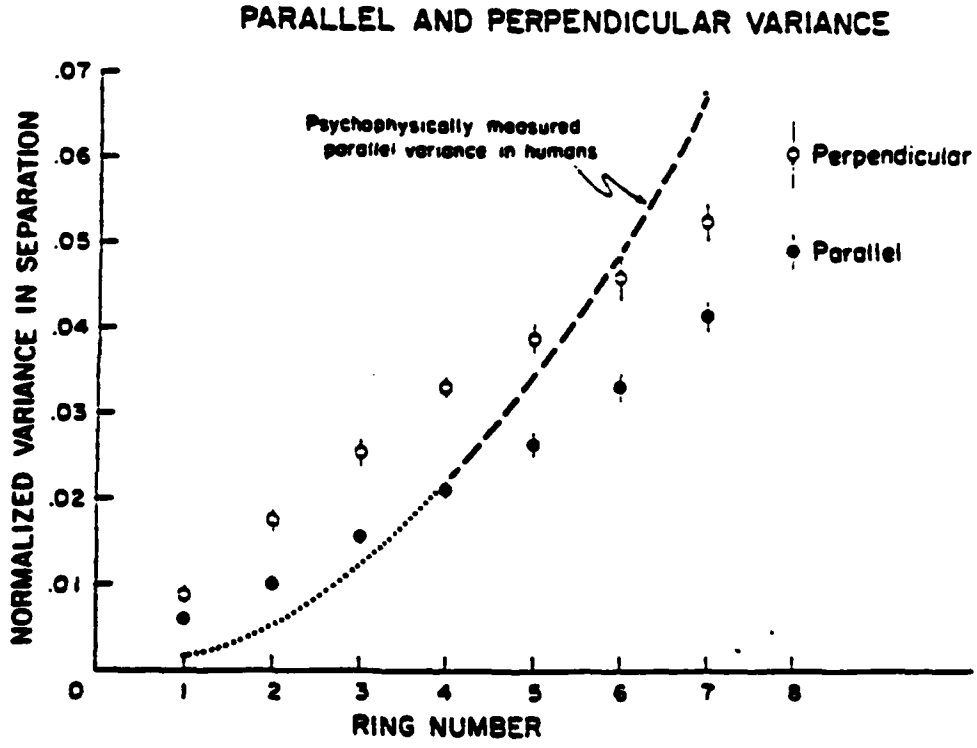
PARALLEL AND PERPENDICULAR VARIANCE
NORMALIZED VARIANCE IN SEPARATION
.07
.06
.05
.04
.03
.02
.01
0
1
2
3
4
5
6
7
8
RING NUMBER
Psychophysically measured parallel variance in humans
Perpendicular
Parallel

Joy Hirsch
F49620-83-C-0026

Figure 8

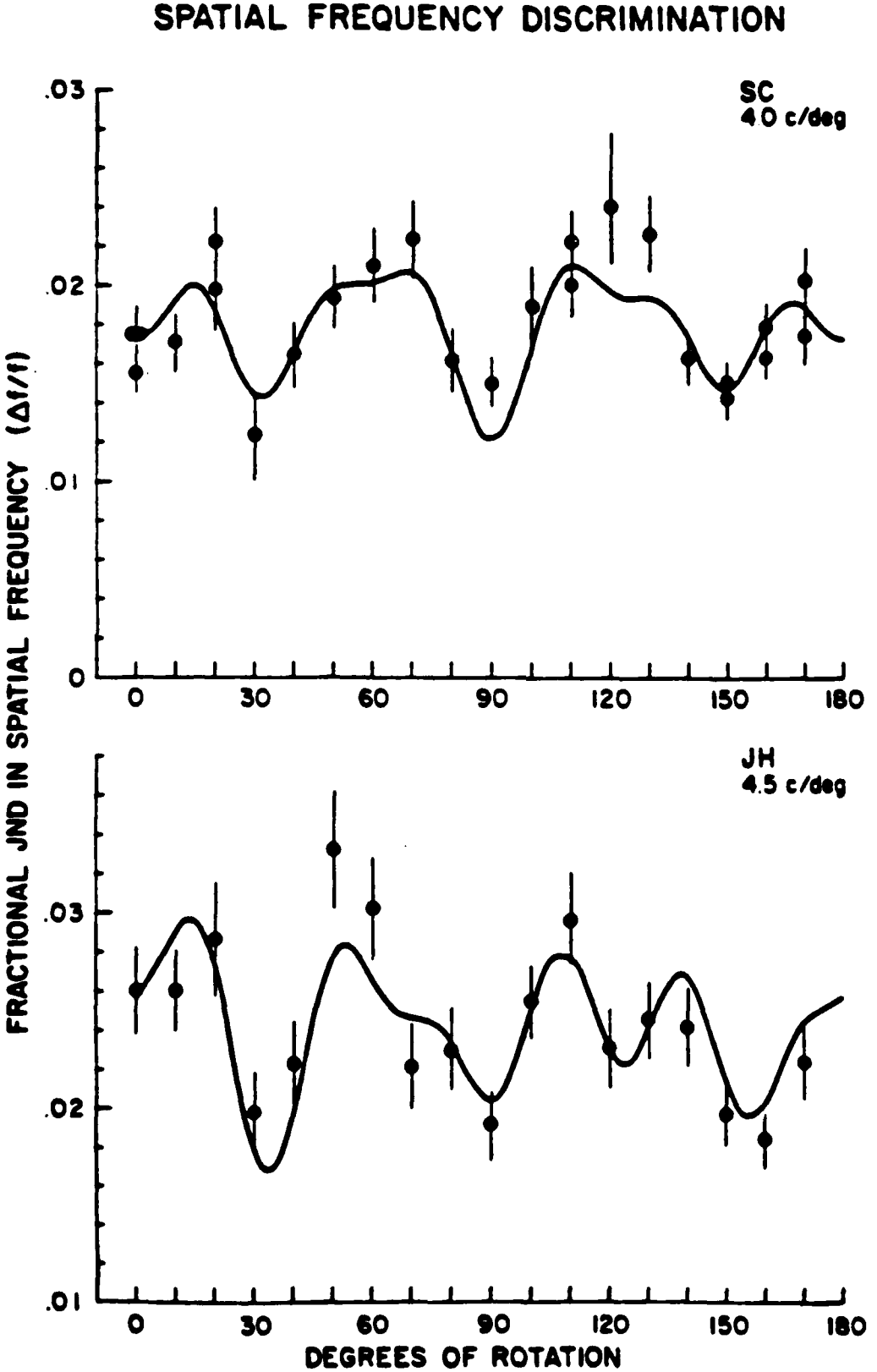

Joy Hirsch
F49620-83-C-0026

Figure 9

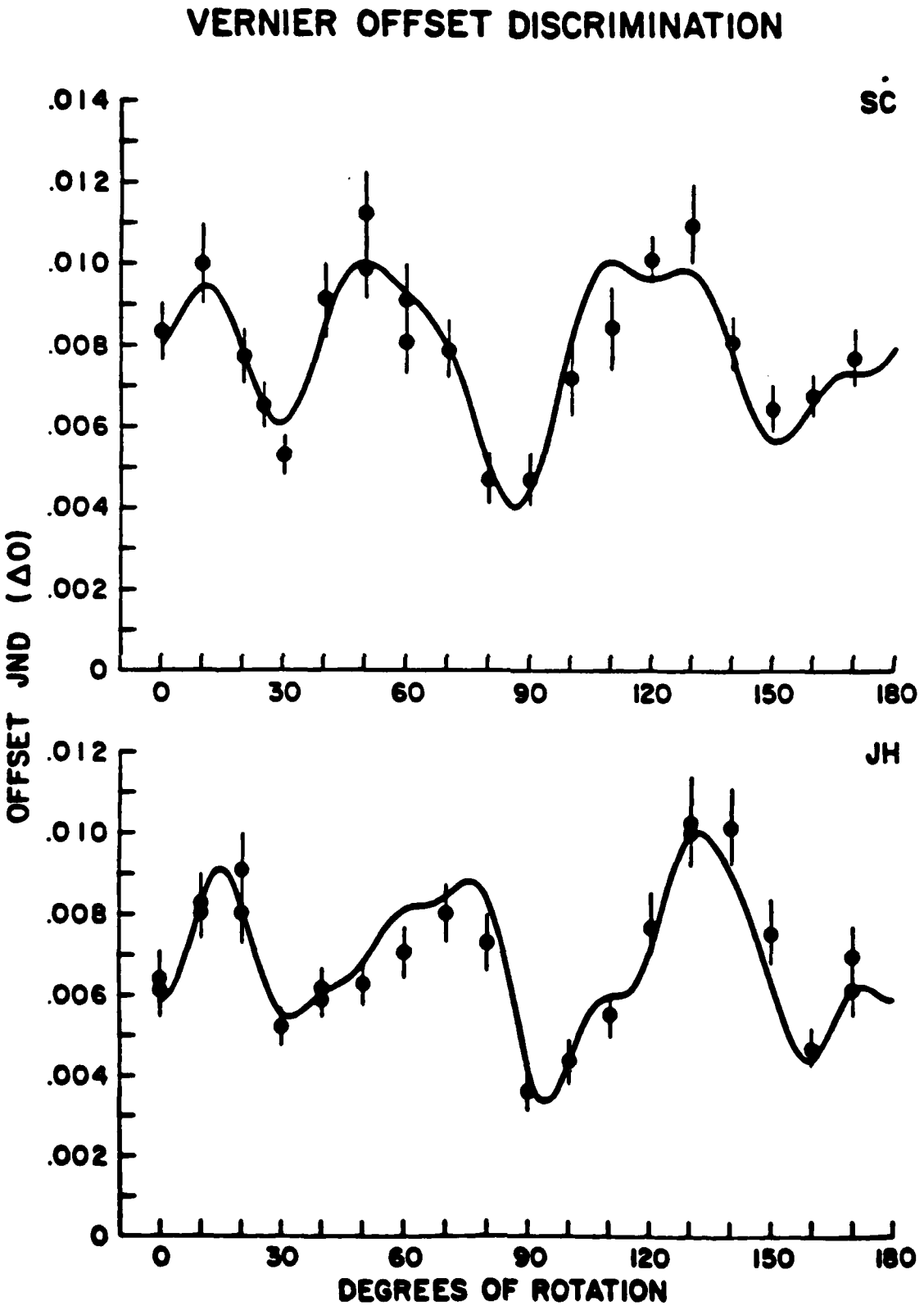

DECOMPOSITION OF ORIENTATION DEPENDENCE

Figure 10

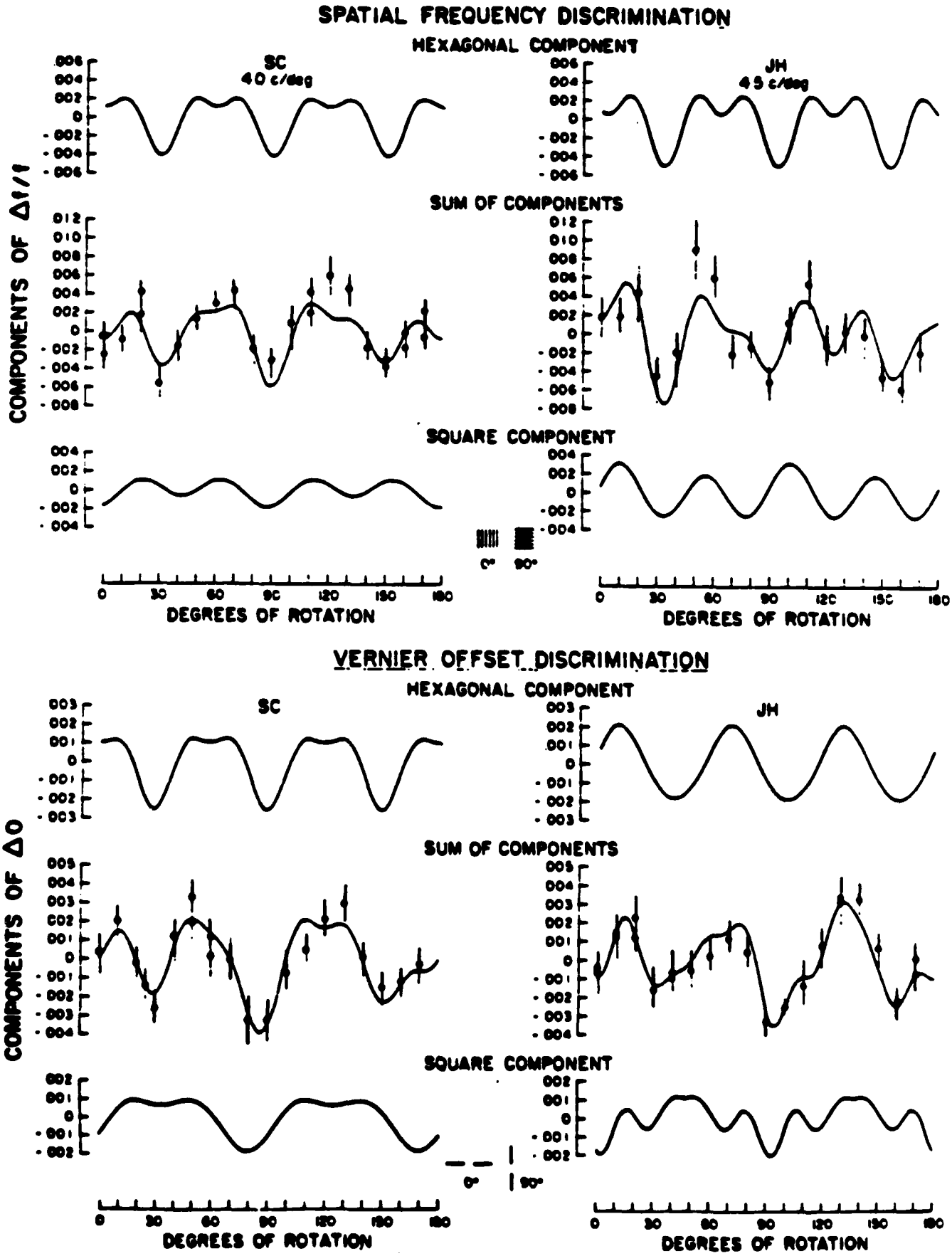

Joy Hirsch
F49620-83-C-0026

Figure 11

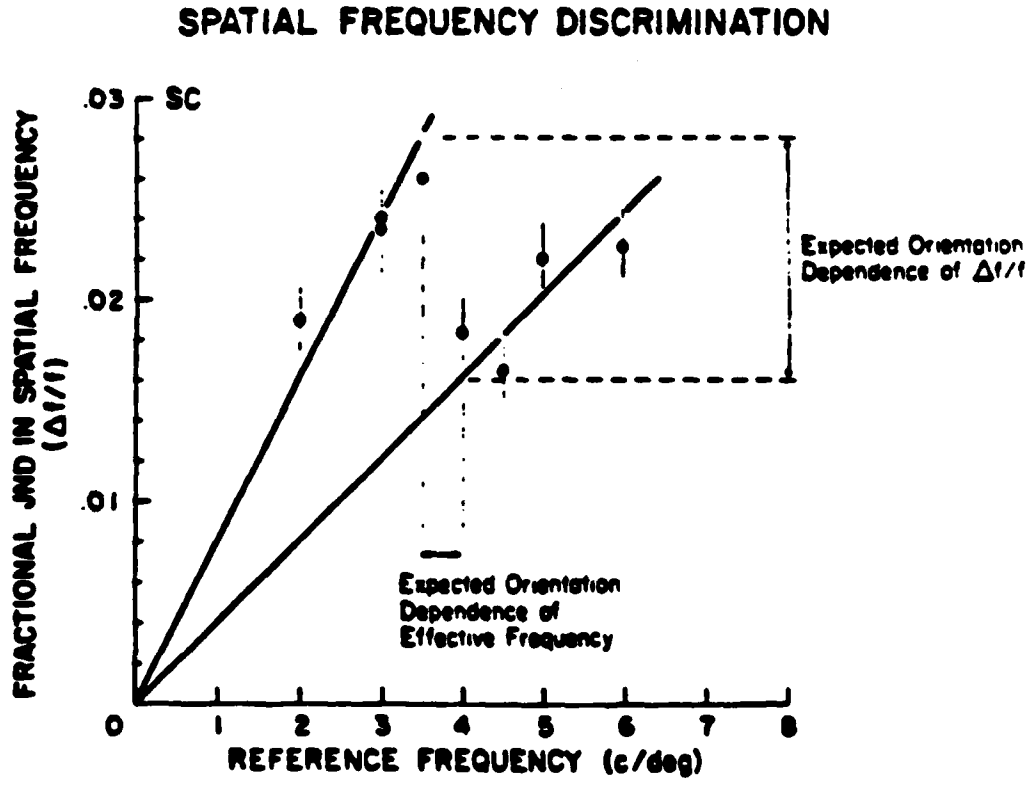

Joy Hirsch
F49620-83-C-0026

LINE GRATING DISCRIMINATION

Figure 12a

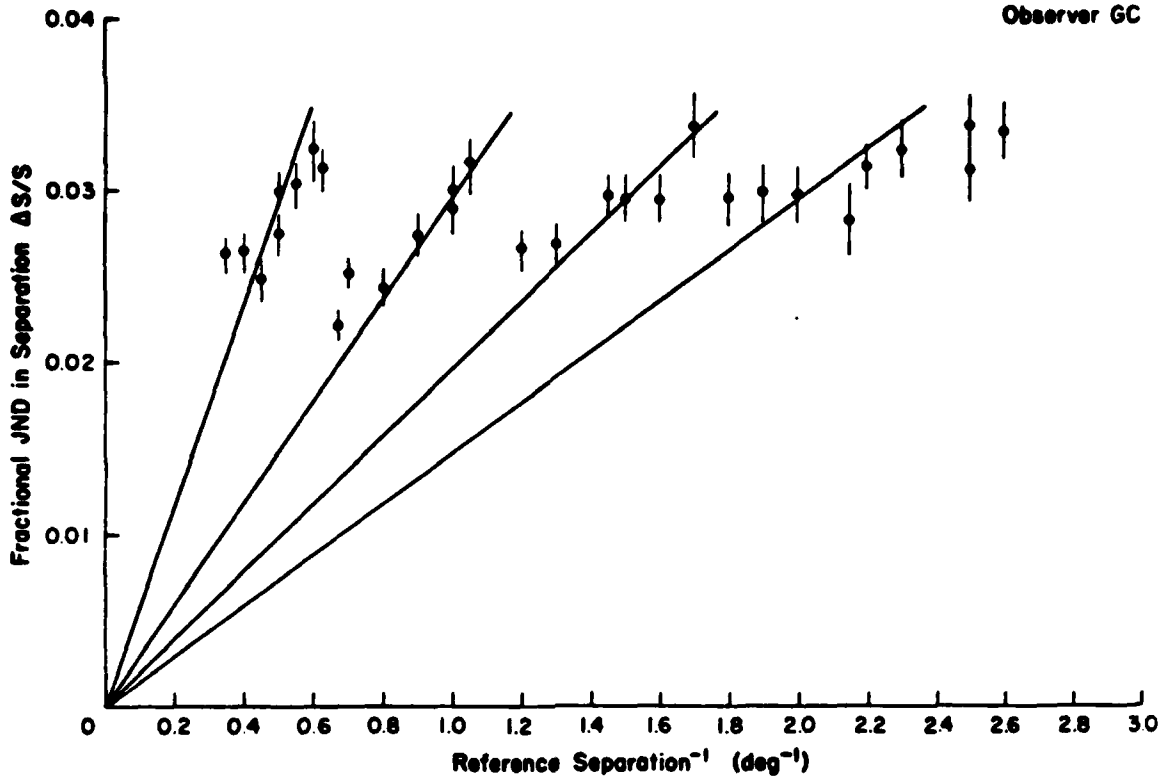

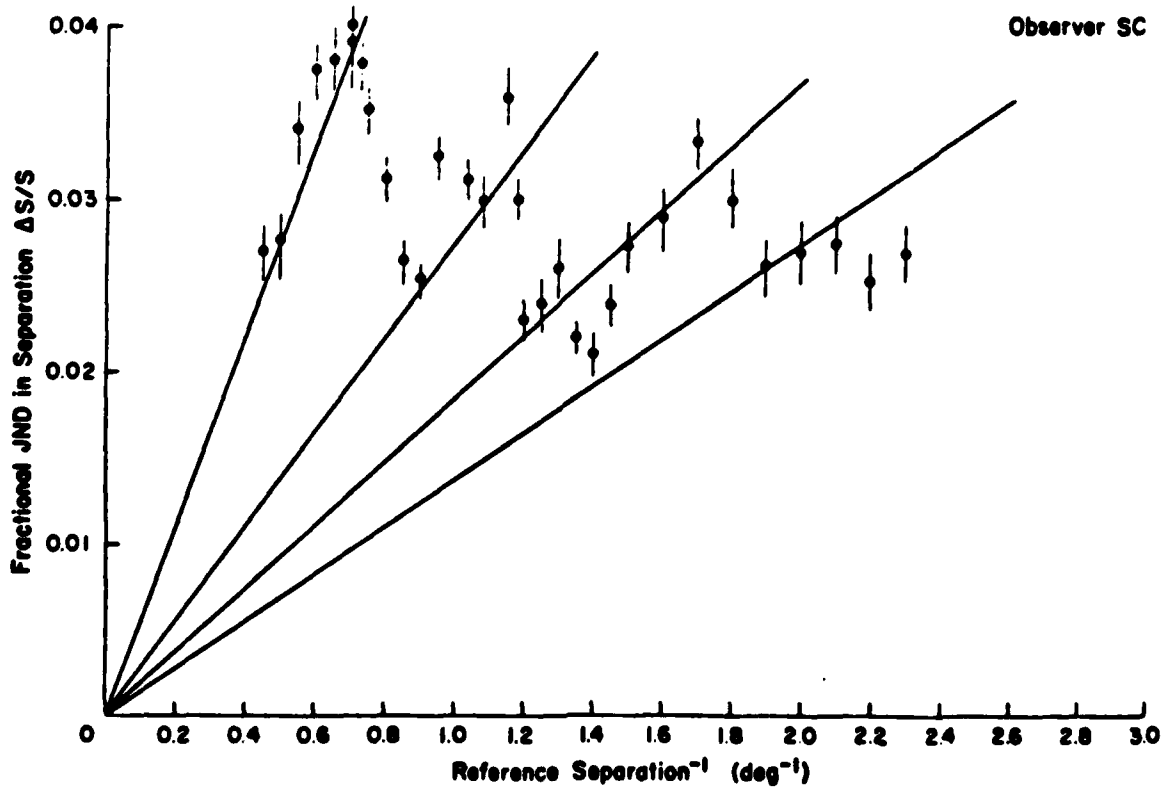

Joy Hirsch
F49620-83-C-0026

LINE GRATING DISCRIMINATION

Figure 12b

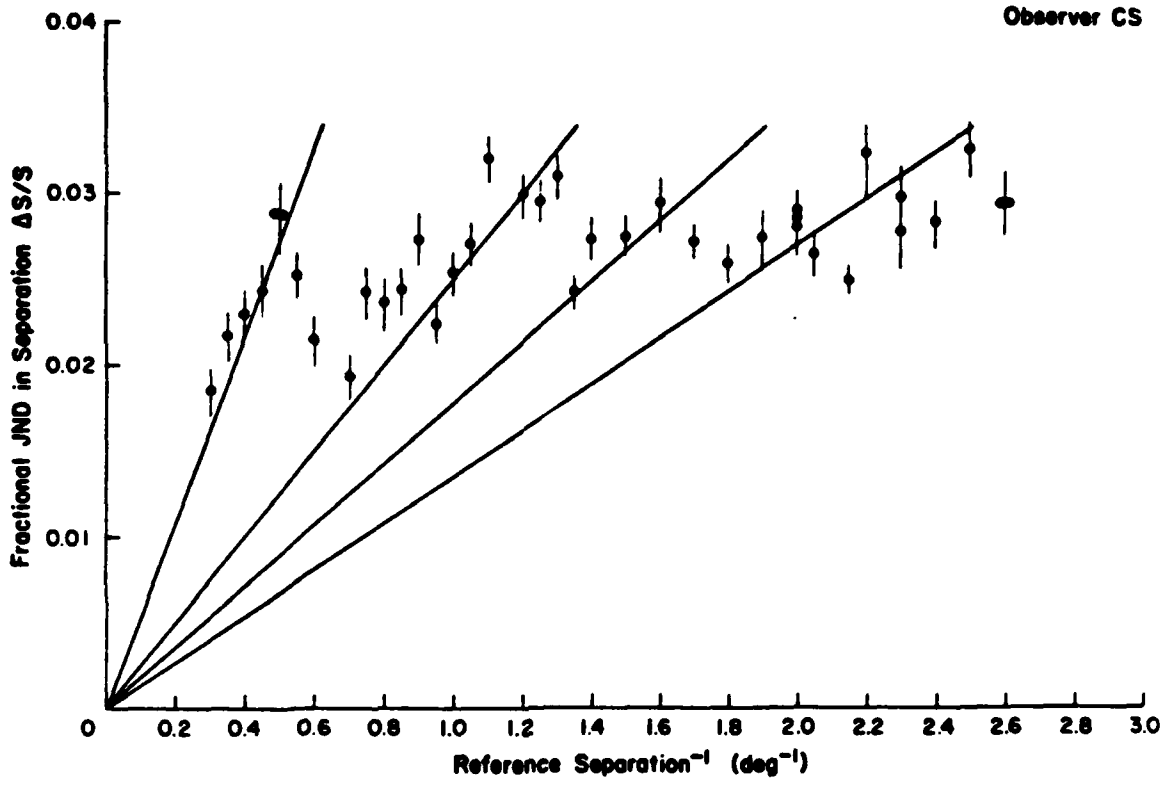

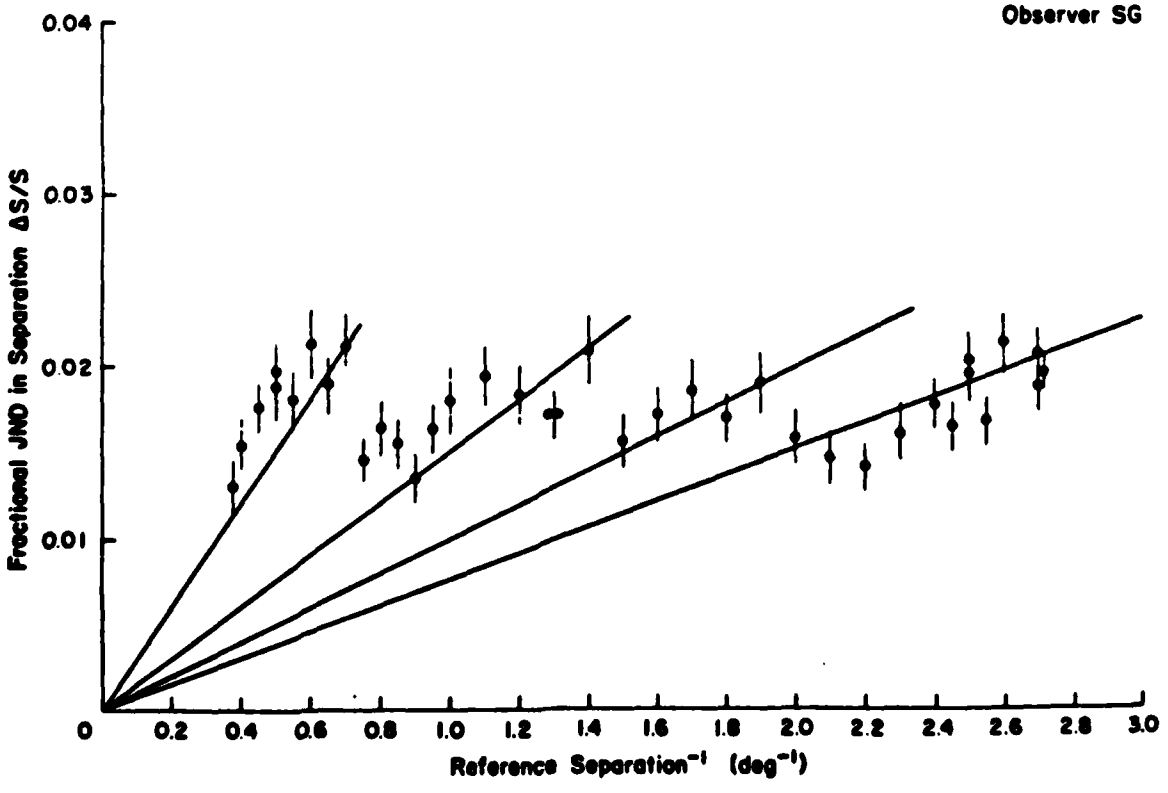

Joy Hirsch
F49620-83-C-0026

Figure 13

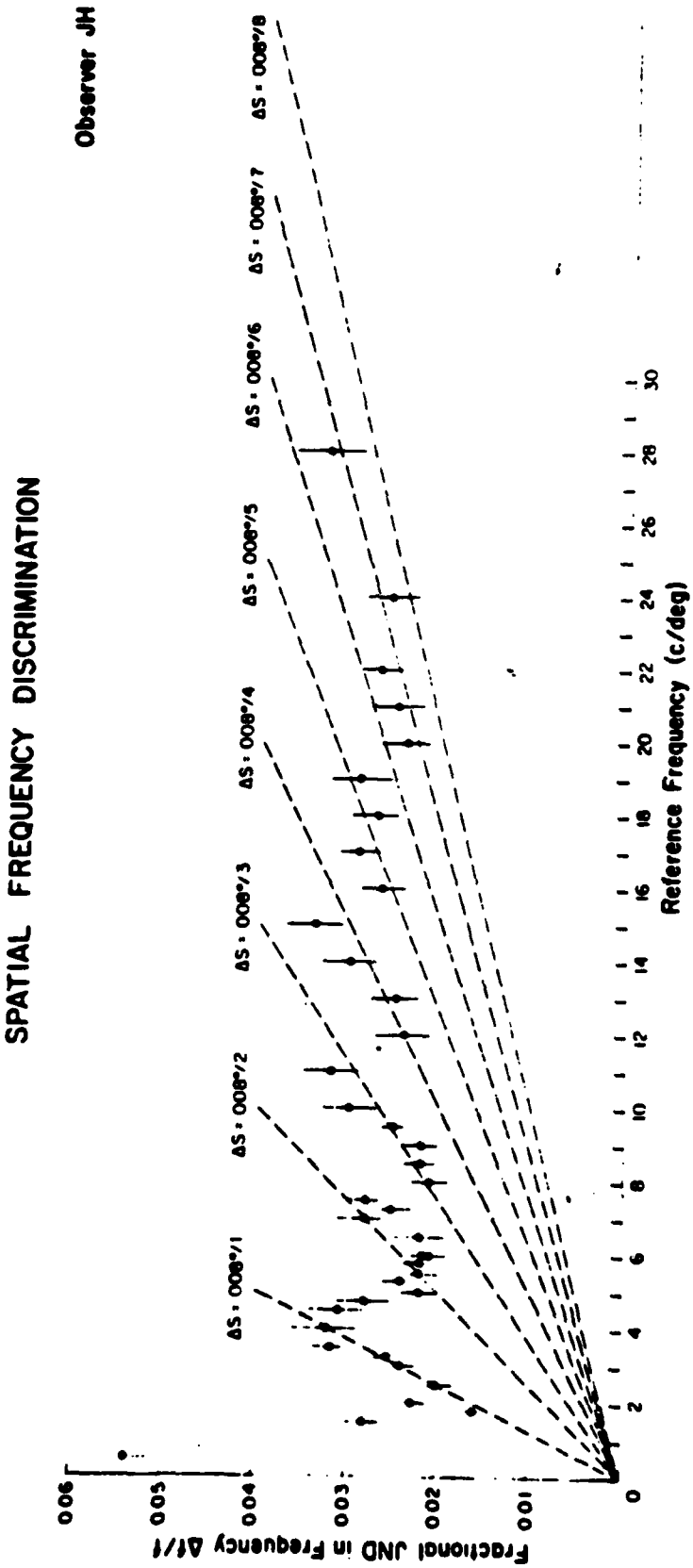

Figure 14

SCHEMATIC MODEL OF POSITION PROCESSING

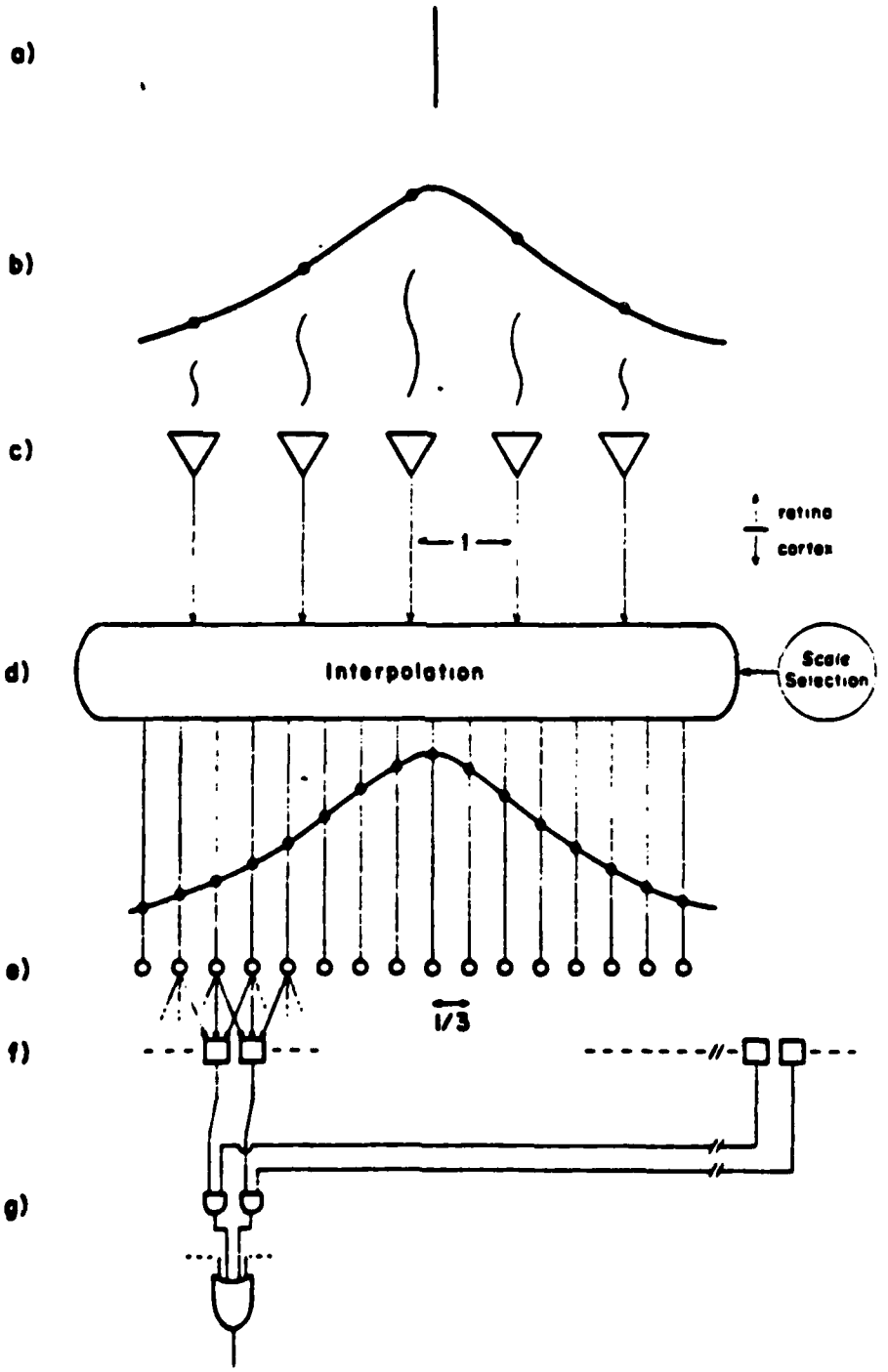

TABLE 1

Parameters of Best Fit Lines

Variance* vs Ring Number

Variance*	Slope	Intercept	X^2	df	Conf.
Uncorrected					
parallel	.0056±.0002	.0001±.0006	8.89	6	.18
perpendicular	.0075±.0003	.0021±.0009	2.60	6	.86

*Variance is expressed in units of mean inter-neighbor distance squared.

TABLE II

Fits to Models of Orientation Dependence

	Observer	Orientation Dependence	X^2	df	conf
Spatial Frequency Discrimination	SC	none	69.5	24	$3x10^{-6}$
	(4.0 c/deg)	hexagonal	33.9	21	.037
		square	67.0	21	$1x10^{-6}$
		hex+square	26.5	18	.088
	JH	none	40.7	17	.001
	(4.5 c/deg)	hexagonal	22.7	14	.065
		square	33.0	14	.003
		hex+square	13.4	11	.270
Vernier Offset Discrimination	SC	none	139.0	20	$<10^{-10}$
		hexagonal	57.5	17	$3x10^{-6}$
		square	96.3	17	$<10^{-10}$
(gap = .25 deg)		hex+square	17.9	14	.210
	JH	none	161.3	23	$<10^{-10}$
		hexagonal	66.6	20	$7x10^{-7}$
		square	125.1	18	$<10^{-10}$
		hex+square	18.4	15	.240

C. PUBLICATIONS

Hirsch, J. and Hylton, R. Limits of spatial frequency discrimination as evidence of neural interpolation. J. Opt. Soc. Am. 72:1367-1374, 1982.

Hirsch, J. and Hylton, R. Quality of the primate photoreceptor lattice and limits of spatial vision. Vision Res. In press, 1983.

Hirsch, J. and Hylton, R. Orientation dependence of visual hyperacuity contains components with hexagonal symmetry. J. Opt. Soc. Am. In press, 1983.

Hirsch, J. and Hylton, R. Spatial frequency discrimination at low frequencies: evidence for position quantization by receptive fields. Submitted, 1983.

Hirsch, J. and Hylton, R. The processing of positional information in the human visual system. Technical Report 8303. Medical Imaging Division, Yale University School of Medicine. 1983.

Hirsch, J. and Hylton, R. Two dimensional sampling by the retinal lattice. Technical Report 8304. Medical Imaging Division. Yale University School of Medicine. 1983.

D. PROFESSIONAL PERSONNEL ASSOCIATED WITH THE RESEARCH EFFORT

1. Joy Hirsch, Principal Investigator
2. John Rose, Systems Analyst
3. Cathryne Stein, Laboratory Assistant
4. Debbie Tewksbury, Word Processing

E. INTERACTIONS

1. Papers presented

Hirsch, J. and Hylton, R. Spatial frequency discrimination of supra-threshold gratings. ARVO, Sarasota, FL, 1982.

Hirsch, J. and Hylton, R. Orientation dependence of hyperacuity contains components with hexagonal symmetry. ARVO Meeting, Sarasota, FL, 1983.

Hirsch, J. and Hylton, R. Quality of the photoreceptor lattice limits spatial vision. Optical Society of America, New Orleans, 1983.

2. Invited Lectures

21 June 1983: University of Texas, Austin, TX -
Quality of the photoreceptor lattice and spatial vision.

23 June 1983: University of Houston, Houston, TX -
A model of visual hyperacuity based on qualities of the photoreceptor lattice.

17 January 1984: University of Rochester, Rochester, N.Y. -
Orientation dependence of visual hyperacuity contains a component with hexagonal symmetry.

1 March 1984: University of Michigan, Dearborn, M.I.
Spatial frequency discrimination of low spatial frequencies.